



1       **Robustness of simulating aerosol climatic impacts using regional model**  
2                         **(WRF-Chem v3.6): the sensitivity to domain size**

3       <sup>1</sup>Xiaodong Wang, <sup>1,2,3</sup>Chun Zhao\*, <sup>1</sup>Mingyue Xu, <sup>1</sup>Qiuyan Du, <sup>1</sup>Jianqiu Zheng, <sup>1</sup>Yun Bi  
4

5  
6       <sup>1</sup>School of Earth and Space Sciences, University of Science and Technology of China, Hefei,  
7 China

8       <sup>2</sup>CAS Center for Excellence in Comparative Planetology, University of Science and Technol  
9 ogy of China, Hefei, China

10       <sup>3</sup>Frontiers Science Center for Planetary Exploration and Emerging Technologies, University  
11 of Science and Technology of China, Hefei, China

12  
13  
14  
15  
16  
17  
18  
19  
20       \*Corresponding authors:     Chun Zhao ([chunzhao@ustc.edu.cn](mailto:chunzhao@ustc.edu.cn))  
21  
22  
23

24       **Key points:**

- 25     1. Domain size has a great influence on the simulated meteorological fields and aerosol  
26     distribution during East Asian summer monsoon (EASM).
- 27     2. Regional simulations with different domain sizes demonstrate consistently that aerosols  
28     weaken EASM moisture transport.
- 29     3. Different domain sizes result in different strength of aerosol-induced changes of temperature  
30     and thus circulation and rainfall over China.

31  
32  
33



34 **Abstract**

35 Domain size can have significant impacts on regional modeling results, but few studies  
36 examining the sensitivities of regional modeling results of aerosol impacts to domain size. This  
37 study investigates the regional modeling sensitivities of aerosol impacts on East Asian summer  
38 monsoon (EASM) to domain size. The simulations with two different domain sizes  
39 demonstrate consistently that aerosols induce the cooling of lower troposphere that leads to the  
40 anti-cyclone circulation anomalies and thus the weakening of EASM moisture transport. The  
41 aerosol-induced adjustment of monsoonal circulation results in a spatial pattern of “+--+” for  
42 precipitation change over the continent of China. Domain size has a great influence on the  
43 simulated meteorological fields. For example, the simulation with increasing domain size  
44 produces weaker EASM circulation, which also affect aerosol distributions significantly. This  
45 leads to the difference of simulated strength and area extent of aerosol-induced changes of  
46 lower-tropospheric temperature and pressure, which further results in different locations of  
47 circulation and precipitation anomalies over the continent of China. For example, over  
48 Southeast China, aerosols induce the increase (decrease) of precipitation from the smaller-  
49 domain (larger-domain) simulation. Different domain sizes simulate consistently aerosol-  
50 induced increase of precipitation around 30°N over East China. This study highlights the  
51 important impacts of domain size on regional modeling results of aerosol impacts on  
52 circulation and precipitation, which may not be limited to East Asia. More generally, this study  
53 also implies that proper modeling of meteorological fields with appropriate domain size is one  
54 of the keys to simulate robust aerosol climatic impacts.

55  
56  
57  
58  
59  
60  
61



## 62 1. Introduction

63 As one of the forcing's of climate change, aerosol contributes the largest uncertainty to  
64 the total radiative forcing estimate, and it has attracted more and more attention since the 1980s  
65 (IPCC, 2013; Li et al., 2019). Aerosols can absorb and scatter solar radiation through Aerosol-  
66 Radiation interactions, affect the regional radiation budget, and amplify its impact through  
67 atmospheric mixing and circulation (e.g., Schwartz, 1996; Rinke et al., 2004; Kim et al., 2007;  
68 Z. Q. Li et al., 2010; C. Zhao et al., 2011, 2012, 2014; Myhre et al., 2013; Kuniyal et al., 2019;  
69 Zhang et al., 2020). Serving as cloud condensation nuclei or ice nuclei, aerosols can change  
70 the microscopic and macroscopic characteristics of clouds and affect the climate, which is  
71 called Aerosol-Cloud interactions (Twomey, 1977; Albrecht, 1989; Ackerman et al., 2000; Fan  
72 et al., 2012, 2013, 2016). And there are many other possible Aerosol-Cloud-Precipitation  
73 processes which may amplify or dampen this effect (Rosenfeld et al., 2008, 2014; Tao et al.,  
74 2012; Fan et al., 2015, 2018).

75 Due to the large population and the rapid economic development, East Asia has  
76 encountered large aerosol loading, and suffered from severe air pollution caused by various  
77 emission sources (e.g., Chan et al., 2008; X. Y. Zhang et al., 2012; Li et al., 2017; An et al.,  
78 2019). Moreover, East Asia is located in the monsoon region, the weather and climate systems  
79 are more complicated, which makes the study of aerosol effects more challenging (Ding et al.,  
80 2005; Ding, 2007; Li et al., 2016, 2019; Wu et al., 2016). In recent decades, the East Asian  
81 summer monsoon (EASM) and summer precipitation in eastern China have shown strong  
82 interdecadal changes (Ding et al., 2008, 2013; Zhou et al., 2009; Zhu et al., 2011; Zhang, 2015),  
83 which had a significant impact on agriculture, economy, and human life (An et al., 2015). Many  
84 factors are related to the interdecadal variability of the EASM, such as extraterrestrial natural  
85 forcing, internal dynamical feedbacks within the climate system and changes in atmospheric  
86 composition (e.g., greenhouse gases and aerosols) and surface conditions (land cover changes  
87 or urbanization) related to anthropogenic factors (Ding et al., 2008,2009; H. M. Li et al., 2010;  
88 Song & Zhou, 2014; Xiao & Duan, 2016; Jiang et al., 2017). As one of the forcing factors of  
89 summer climate change in East Asia, aerosol have attracted many people to study the weather  
90 and climate effects of summer aerosols in East Asia (Cowan & Cai, 2011; H. Zhang et al., 2012;  
91 Guo et al., 2013; Jiang et al., 2013, 2017; Wu et al., 2013; Song et al., 2014; Li et al., 2015,  
92 2018; Wang et al., 2015, 2017; Chen et al., 2016; Kim et al., 2016; Xie et al., 2016; Dong et  
93 al., 2019).



94 Numerous studies have used global climate models to study the impacts of  
95 anthropogenic aerosols on the EASM climate and understand the mechanisms underneath (e.g.,  
96 Guo et al., 2013; Jiang et al., 2013, 2017; Song et al., 2014; Yan et al., 2015; Chen et al., 2016;  
97 Wang et al., 2017; Li et al., 2018; Dong et al., 2019). The global modeling results have shown  
98 that aerosols tend to reduce the land-sea thermal contrast, weaken the EASM, and thereby  
99 reduce the rainfall over the continent (e.g., Guo et al., 2013; Jiang et al., 2013; Song et al., 2014;  
100 Wang et al., 2017; Li et al., 2018; Dong et al., 2019). The reduction of monsoon precipitation  
101 over the continent may reduce the release of latent heat from condensation in the upper  
102 troposphere and further weaken the East Asian summer monsoon (e.g., Jiang et al., 2013; Li et  
103 al., 2019). Jiang et al. (2013) used the CAM5 (the Community Atmospheric Model version 5)  
104 model to study the effect of different aerosol types on East Asian summer clouds and  
105 precipitation, and found that all anthropogenic aerosols suppressed precipitation in North China  
106 and enhanced precipitation in South China and adjacent ocean areas. Through analyzing the  
107 CMIP5 (Coupled Model Intercomparison Program phase 5) modeling results, Song et al. (2014)  
108 examined the contributions of different forcings (aerosol forcing, greenhouse gas forcing,  
109 natural forcing) to the weakening of EASM circulation during 1958–2001, and found that  
110 aerosol forcing plays a major role in the weakening of EASM, and the contribution of natural  
111 forcing is almost negligible, and the forcing of greenhouse gases is conducive to slightly  
112 strengthening rather than weakening the monsoon circulation.

113 Global climate models have been widely used for investigating aerosol impacts,  
114 however, there are still large uncertainties with the results at regional scale partly because the  
115 regional-scale monsoon rainband and aerosol distributions are still not able to be described  
116 accurately with relatively lower model horizontal resolution (H. M. Li et al., 2010; Guo et al.,  
117 2013; Jiang et al., 2013; Song et al., 2014; Li et al., 2018; Dong et al., 2019). In comparison,  
118 regional model often has higher horizontal resolution and can better capture regional features  
119 of weather and climate systems and aerosol distributions, and therefore has been used to  
120 investigate aerosol climatic impacts recently (e.g., Zhao et al., 2011, 2012; Wu et al., 2013;  
121 Wang et al., 2015; Zhuang et al., 2018). For example, using the regional model (RegCCMS),  
122 Wang et al. (2015) found that aerosol-cloud interaction decreases the autoconversion rates of  
123 cloud water to rain water and increases the liquid water path of clouds in East China,  
124 strengthens the cooling of lower atmosphere caused by the direct radiation effect, and  
125 suppresses the convective precipitation. Wu et al. (2013), with the regional model (WRF-  
126 Chem), found that the aerosol heating effect caused the cloud to move northward over East  
127 China and led to the increased precipitation in the north.



128           Although regional model at higher horizontal resolution may better capture regional  
129 features of wind, cloud, precipitation, and aerosol, it also introduces additional uncertainties  
130 on modeling regional aerosol climatic impacts resulted from the lateral boundary of regional  
131 simulation. Previous studies have found that domain size of regional model can significantly  
132 influence the simulation results (e.g., Warner et al., 1997; Leduc and Laprise, 2009; Leduc et  
133 al., 2011; Bhaskaran et al., 2012; Giorgi, 2019). For example, Bhaskaran et al. (2012) studied  
134 the sensitivity of the simulated hydrological cycle to the regional domain size over the Indian  
135 subcontinent. They found that the simulations with smaller domains produced increased  
136 precipitation and evapotranspiration on seasonal mean and higher number of moderate  
137 precipitation days relative to the ones with larger domains. Different distributions of cloud,  
138 precipitation, and winds from the simulations with different domain sizes may lead to different  
139 aerosol distributions and its climatic impacts. Previous studies have found that aerosol impacts  
140 on precipitation, clouds, and circulation will be significantly different under different weather  
141 and climate conditions (e.g., Wu et al., 2013; Wang et al., 2015; Xie et al., 2016). In addition,  
142 Seth and Giorgi. (1998) found that the smaller-domain simulation produced better precipitation  
143 compared with the observations, but resulted in an unrealistic response to the internal forcing.  
144 This indicates that the simulation domain size may also affect the aerosol impacts on large-  
145 scale circulation. Therefore, the regional simulation with increased domain size may be  
146 preferred to better reflect the overall aerosol impacts on large-scale circulation and weather  
147 system without the strict constraint from the boundary forcing (e.g., Seth and Giorgi, 1998;  
148 Leduc and Laprise, 2009; Xue et al., 2014), but the increased domain size may make the  
149 simulations deviated from the forcing such as the reanalysis.

150           As far as we know, there are few studies examining the sensitivities of regional  
151 modeling results of aerosol impacts to regional domain size. Although it can be expected that  
152 domain size will play a role, it is not known to what extent and how domain size can affect  
153 modeling results of aerosol climatic impacts. Therefore, in this study, the regional online-  
154 coupled meteorology and chemistry model WRF-Chem (Weather Research and Forecasting  
155 model coupled with Chemistry) (Grell et al., 2005; Skamarock et al., 2008) is used to study the  
156 aerosol impacts on East Asian summer monsoon system and focus on the modeling sensitivities  
157 to regional domain size. WRF-Chem has been widely used for studying aerosol meteorological  
158 and climatic impacts over East Asia (e.g., A. J. Ding et al., 2013; Wu et al., 2013; Gao et al.,  
159 2014; Chen et al., 2014; Zhao et al., 2014; Huang et al., 2016; Liu et al., 2016; Petaja et al.,  
160 2016; Zhao B et al., 2017). The investigation of aerosol impacts under different simulated  
161 meteorological fields due to different domain sizes may also help understand the different



162 modeling results about the aerosol impacts on East Asian summer monsoon from previous  
163 studies. The study is organized as follows. Section 2 describes the numerical experiments and  
164 methods. The results and discussions are presented in Section 3. A summary is provided in  
165 Section 4.

166

## 167 **2. Methodology**

### 168 **2.1 WRF-Chem**

169 In this study, the version of WRF-Chem updated by the University of Science and  
170 Technology of China (USTC version of WRF-Chem) is used. The model simulates the  
171 emission, transport, mixing, and chemical transformation of trace gases and aerosols  
172 simultaneously with the meteorology, and can be used for investigation of regional-scale air  
173 quality and interactions between meteorology and chemistry. Compared with the publicly  
174 released version, the USTC version of WRF-Chem includes a few additional functions, such  
175 as the diagnosis of radiative forcing of aerosol species, optimized Kain-Fritsch (KF) convection  
176 scheme, aerosol-snow interaction, land surface coupled biogenic Volatile Organic Compound  
177 (VOC) emission, etc. (Zhao et al., 2013a, b, 2014, 2016; Hu et al., 2019; Du et al., 2020), all  
178 of which may have important impact on modeling aerosol and its climatic impacts.

179 The Model for Simulating Aerosol Interactions and Chemistry (MOSAIC) aerosol  
180 module coupled with CBM-Z (carbon bond mechanism) photochemical mechanism in WRF-  
181 Chem is selected in this study (Zaveri & Peters, 1999; Zaveri et al., 2008). MOSAIC uses a  
182 sectional approach to represent aerosol size distributions with four or eight discrete size bins  
183 in the current version of WRF-Chem (Fast et al., 2006). To reduce the computational cost, four  
184 discrete size bins is selected in this study. All major aerosol components including sulfate,  
185 nitrate, ammonium, black carbon, organic matter, sea-salt, mineral dust, and other inorganic  
186 matter (OIN) are simulated in the model. The MOSAIC aerosol scheme includes physical and  
187 chemical processes of nucleation, condensation, coagulation, aqueous-phase chemistry, and  
188 water uptake by aerosols. Dry deposition of aerosol mass and number is simulated following  
189 the approach of Binkowski and Shankar (1995), which includes both turbulent diffusion and  
190 gravitational settling. Wet removal of aerosols by grid-resolved stratiform clouds and  
191 precipitation includes in-cloud removal (rainout) and below-cloud removal (washout) by  
192 impaction and interception, following Easter et al. (2004) and Chapman et al. (2009). In this  
193 study, cloud-ice-borne aerosols are not explicitly treated in the model, but the removal of  
194 aerosols by the droplet freezing process is considered. Convective transport and wet removal



195 of aerosols by cumulus clouds is coupled with the Kain-Fritsch cumulus scheme as Zhao et al.  
196 (2013b). Aerosol radiative feedback is coupled with the Rapid Radiative Transfer Model  
197 (RRTMG) (Mlawer et al., 1997; Iacono et al., 2000) for both SW and LW radiation as  
198 implemented by Zhao et al. (2011). The optical properties and direct radiative forcing of  
199 individual aerosol species in the atmosphere are diagnosed following the methodology  
200 described in Zhao et al. (2013a).

201

## 202 **2.2 Numerical experiments**

203 Four sets of experiments CTRL-L, CTRL-S, CLEAN-L, CLEAN-S with different  
204 simulation domain sizes or emission configurations are conducted as listed in Table 1. The  
205 control (CTRL-S, CTRL-L) simulations use standard anthropogenic emission dataset  
206 (described in Section 2.3), while the clean simulations (CLEAN-S, CLEAN-L) apply a factor  
207 of 0.1 on the standard emissions within the small domain to represent a clean atmosphere  
208 condition over East Asia (Fig. 1). The CTRL-L and CTRL-S (CLEAN-L and CLEAN-S)  
209 represent the simulations with large and small domain sizes, respectively, as shown in Figure  
210 1. The aerosol impacts can be calculated by the difference between the CTRL and CLEAN  
211 simulations for each simulation domain. The comparison of aerosol impacts between the large  
212 and small simulation domains implies the sensitivity of aerosol impacts to domain size.

213 All the WRF-Chem experiments select the Morrison two-moment microphysics  
214 (Morrison et al., 2009), Kain-Fritsch cumulus scheme (Kain, 2004), unified Noah land-surface  
215 model, Rapid Radiative Transfer Model (RRTMG) longwave and shortwave radiation schemes  
216 (Iacono et al., 2008), and MYNN planetary boundary layer (PBL) scheme (Nakanishi & Niino,  
217 2006,2009). Following Du et al. (2020), the PBL mixing coefficient is modified to simulate  
218 better PBL mixing of aerosols. Five ensemble simulations are performed for each experiment  
219 by changing the initial conditions at UTC 0000 from May 12 to May 16, 2017. The averaged  
220 results from five ensembles are analyzed to reduce the influence of modeling internal  
221 variability. The simulations run through entire June and July of 2017. The analysis focuses on  
222 the simulation results for June 1 to July 31, 2017. The meteorological initial and lateral  
223 boundary conditions are derived from National Centers for Environmental Prediction (NCEP)  
224 Final (FNL) Operational Global Analysis data (NCEP, 2000) with a resolution of  $1^\circ \times 1^\circ$  and a  
225 time resolution of 6h. The chemical initial and boundary conditions are provided by a quasi-  
226 global WRF-Chem simulation for the same time period. The quasi-global WRF-Chem  
227 simulation is performed at  $1^\circ \times 1^\circ$  horizontal resolution with  $360 \times 130$  grid cells ( $180^\circ$ W-  
228  $180^\circ$ E,  $60^\circ$ S- $70^\circ$ N). More details about the general configuration of a quasi-global WRF-Chem



229 simulation can be found in Zhao et al. (2013b) and Hu et al. (2016). The simulation  
230 configuration is summarized in Table 2.

### 231 **2.3 Emissions**

232 Biomass burning emissions are obtained from the Fire Inventory (FINN) of the National  
233 Center for Atmospheric Research with hourly temporal resolution and 1 km horizontal  
234 resolution (Wiedinmyer et al., 2011), and the injection heights follow Dentener et al. (2006)  
235 for the Aerosol Comparison between Observations and Models (AeroCom) project. The natural  
236 dust emission fluxes are calculated based on the adjusted GOCART dust emission scheme  
237 (Ginoux et al., 2001; Zhao et al., 2010), and the emitted dust particles are distributed into the  
238 MOSAIC aerosol size bins following a theoretical expression based on the physics of scale-  
239 invariant fragmentation of brittle materials derived by Kok (2011). More details about the dust  
240 emission scheme coupled with MOSAIC aerosol scheme in WRF-Chem can be found in Zhao  
241 et al. (2010, 2013b). Sea-salt emission follows Zhao et al. (2013a), which includes correction  
242 of particles with radius less than 0.2  $\mu\text{m}$  and dependence of sea-salt emission on sea surface  
243 temperature. Anthropogenic emissions are obtained from the Multi-resolution Emission  
244 Inventory for China (MEIC) at  $0.1^\circ \times 0.1^\circ$  horizontal resolution and with monthly temporal  
245 resolution for 2015 (Li et al., 2017; Zheng et al., 2018), except that the emissions outside of  
246 China are from the Hemispheric Transport of Air Pollution version2 (HTAPv2) at  $0.1^\circ \times 0.1^\circ$   
247 horizontal resolution and with monthly temporal resolution for the year 2010 (Janssens-  
248 Maenhout et al., 2015) (Fig. 1). As discussed above, the anthropogenic emissions in the  
249 CLEAN experiments is a factor of 0.1 of that in the CTRL experiment, and in the CLEAN-L  
250 experiment, only the emissions in the area of the small domain (denoted by the red box) are  
251 adjusted. In this way, the emission reduction from the simulations with both domains are made  
252 consistent.

253

## 254 **3. Results**

### 255 **3.1 Sensitivity of simulated meteorological fields to domain size**

256 Figure 2 shows the spatial distributions of precipitation and moisture transport at 700  
257 hPa over the small domain averaged for June and July of 2017 from the observation and  
258 reanalysis, and the simulations of CLEAN-S and CLEAN-L. The observation and reanalysis  
259 show that the southwesterly transports large amount of moisture into East China. The converge  
260 of large amount of moisture results in heavy precipitation over southern China and its adjacent  
261 ocean. Due to the gradual weakening of northeastward moisture transport and the blocking





262 effect of the western mountains, precipitation becomes much weaker over northern and western  
263 China. Compared with the CMORPH observation and ERA5 reanalysis (Fig. 2), CLEAN-S  
264 can reasonably produce the spatial distribution of precipitation and moisture transport at 700  
265 hPa, with slight underestimation of meridional moisture transport over eastern China. It is  
266 evident that the meridional moisture transport over southern China becomes weaker with the  
267 increasing domain size, and the eastward transport becomes stronger. In addition, the overall  
268 southwesterly moisture transport shift to the east. This leads to a decrease of precipitation over  
269 eastern China and an increase over the East China Sea. Compared with the observations of  
270 hourly precipitation from the CMA stations over eastern China (Fig. S1 in the supporting  
271 material), both the CLEAN-S and CLEAN-L experiments can generally reproduce the daily  
272 variation of precipitation over eastern China, although the CLEAN-L simulated precipitation  
273 is lower consistent with its weaker moisture transport over the region.

274 The difference in moisture transport between the simulations with different domain  
275 sizes results from their difference in geopotential height and wind circulation. Figure 3 shows  
276 the spatial distributions of geopotential height (GPH) and wind field at 700 hPa from the  
277 CLEAN-S simulation, and the difference between CLEAN-L and CLEAN-S. The comparison  
278 with the ERA5 reanalysis shows that the CLEAN-S can well simulate the distributions of GPH  
279 and wind fields at 700 hPa (Fig. S2 in the supporting material). The spatial distribution of wind  
280 fields is generally consistent with that of moisture transport (Fig. 2), and is largely controlled  
281 by the West Pacific sub-tropical high (WPSH). Compared to CLEAN-S, CLEAN-L simulates  
282 lower GPH at 700 hPa and produces an anomalous lower pressure center on the East China  
283 Sea, which indicates the weaker WPSH with increasing domain size. This causes the  
284 southwestward wind anomalies over the continent, which weakens the monsoon driven  
285 northeastward moisture transport. Over the South China Sea, the westerly anomalies enhance  
286 the eastward transport of moisture.

287 The impact of domain size is not only on the horizontal distribution of wind fields but  
288 also on the vertical circulation. Figure 4 shows the cross-section of meridional temperature  
289 anomalies and wind averaged for 105°E and 122°E from the CLEAN-S simulation, and the  
290 difference of temperature (not meridional temperature anomalies) and wind between CLEAN-  
291 L and CLEAN-S. The meridional temperature anomalies are calculated by subtracting the  
292 mean temperature in this latitude range (as shown in Fig. 4) at each pressure level. First of all,  
293 CLEAN-S can general reproduce the temperature gradient and wind circulation from the ERA5  
294 reanalysis (Fig. S3 in the supporting material). Relatively large meridional temperature  
295 gradient exists between 700 hPa and 200 hPa, where the temperature is higher over the South.



296 Below 700 hPa, the temperature gradient is relatively weaker, and the temperature is higher  
297 over the North. Along with this distribution of temperature gradient, meridional wind blows  
298 from the South and the North and converges at the latitude around 34°N, which generates  
299 strong upward motion in the area of 20°N-35°N. This is consistent with the spatial distribution  
300 of precipitation and moisture transport (Fig. 2). Compared with the CLEAN-S experiment, the  
301 CLEAN-L experiment produces larger meridional temperature gradient between 700 hPa and  
302 200 hPa and weaker gradient below 850 hPa. The circulation from the CLEAN-L is generally  
303 consistent with CLEAN-S, but the southerly wind from CLEAN-L is weaker and the northerly  
304 wind is stronger. This results in an overall northerly wind anomalies from CLEAN-L compared  
305 with CLEAN-S, and also a southward shift of the wind convergence from 34°N to 32°N. It is  
306 also noteworthy that the upward motion is weakened around 22°N-38°N and strengthened to  
307 the south of 20°N due to the increased domain size.

308

### 309 **3.2 Sensitivity of simulated aerosol characteristics to domain size**

310 Figure 5 shows the spatial distribution of AOD averaged for June and July of 2017 from  
311 the CTRL-S simulation, and the difference between CTRL-L and CTRL-S. It can be seen that  
312 relatively high AOD (>0.6) exists in the Sichuan Basin and the North China Plain. The AOD  
313 over East Central China and South China is relatively lower (0.2-0.5), which is in line with  
314 previous research (Luo et al., 2014; Qi et al., 2013). In general, the CTRL-S generally captures  
315 the spatial distribution of retrieved AOD from MISR (Fig. S4 in the supporting material).  
316 Compared with the CTRL-S experiment, CTRL-L simulates a similar spatial pattern of AOD  
317 as CTRL-S, but produces higher AOD in southern China and lower AOD in most areas of  
318 northern China. To explore the reasons of difference between the two simulations, Figure 6  
319 shows the spatial distributions of column integrated total PM<sub>2.5</sub> concentration and water  
320 content in aerosol averaged for June and July of 2017 from the CTRL-S simulation, and the  
321 difference between CTRL-L and CTRL-S. The CTRL-S simulation shows high PM<sub>2.5</sub> mass  
322 loading over North China Plain, which is consistent with the spatial distribution of AOD (Fig.  
323 5). The PM<sub>2.5</sub> mass loading also shows high values over Northwest China, which is not shown  
324 in the spatial distribution of AOD. This is mainly due to the high mass loading of dust over  
325 Northwest China (Fig. S5 in the supporting material), and the water content associated with  
326 dust is relatively small.

327 CTRL-L simulates higher PM<sub>2.5</sub> mass loading over Southeast China and lower values  
328 over North China, which is consistent with AOD. The difference of water content in aerosol  
329 shows similar pattern. The analysis shows that the difference of PM<sub>2.5</sub> mass loading over



330 North China is mainly due to the difference of dust, while the difference over Southeast China  
331 is due to anthropogenic aerosols (Fig. S5). The reduction of dust mass loading over North  
332 China from CTRL-L is primarily due to its weakening of westerlies over Northwest China  
333 compared to CTRL-S (Fig. 3), which results in less transport of dust into the downwind region.  
334 The increase of aerosol mass loading over Southeast China in CTRL-L is partly due to its less  
335 wet scavenging associated with weak precipitation (Fig. 2). The weakening of northward  
336 transport of aerosol (Fig. 3) also contributes to the increase of PM<sub>2.5</sub> mass loading over  
337 southern China in CTRL-L. Besides the change of dry aerosol mass loading, the change of  
338 water content in aerosol between the two experiments also contributes to the change in AOD,  
339 which results from the difference of both dry aerosol mass and moisture.

340 Figure 7 shows the latitude-height cross-section of total PM<sub>2.5</sub> averaged between  
341 105°E and 122°E for June and July of 2017 from the CTRL-S experiment, and the difference  
342 between CTRL-L and CTRL-S. The latitudinal distribution of aerosol is consistent with its  
343 spatial pattern with high aerosol mass concentration over North China. The mass concentration  
344 gradually reduces from the surface to the free atmosphere. The mass concentration around 500  
345 hPa over North China can reach 5 ug/m<sup>3</sup> that is comparable to the surface concentration over  
346 South China. In general, CTRL-L simulates higher aerosol mass concentration over South  
347 China and lower aerosol mass concentration over North China from the surface to about 500  
348 hPa. At 32°N-36°N, CTRL-L simulates lower aerosol mass concentration near the surface and  
349 higher above 850 hPa. The difference of aerosol horizontal and vertical distributions and also  
350 the circulation patterns between the two experiments may lead to the difference in simulating  
351 aerosol impacts on East Asian monsoon system.

352

### 353 3.3 Sensitivity of aerosol impact to domain size

354 Before studying the sensitivity of aerosol impacts to domain size, the impacts of aerosol  
355 on precipitation and circulation from the small domain simulations are first investigated. Figure  
356 8 shows the spatial distributions of aerosol-induced difference (CTRL-CLEAN) of  
357 precipitation and moisture transport at 700 hPa averaged for June and July of 2017 from the  
358 small domain simulations. The dominant effect is that aerosol weakens the southwesterlies  
359 flow and reduces the moisture transport over the continent of Central and South China  
360 (primarily between 105°E-115°E). Along the coast of Southeast China, the moisture transport  
361 is enhanced slightly. Over the continent of China, aerosol induces a “+--+” pattern of  
362 precipitation changes, i.e., precipitation increases in the south of 25°N, north of 40°N, and  
363 around 30°N, while decreases at 25°N~30°N and 32°N~40°N. This weakening of monsoonal



364 circulation at the lower troposphere is found mainly due to the cooling of lower troposphere  
365 and thus the increase of surface pressure by aerosols (Fig. 9). The temperature averaged for  
366 lower troposphere (below 500 hPa) is reduced by aerosols over the continent of China, which  
367 results in a positive pressure anomaly center in Southwest China. This leads to an anticyclone  
368 anomaly as shown in Fig. 8, which weakens the monsoonal southwesterlies between 105°E-  
369 115°E.

370 In order to further understand the mechanisms of aerosol impacts and isolate aerosol-  
371 radiation and aerosol-cloud interactions, another set of numerical experiment (NoRA-S) with  
372 the small domain are conducted, similar as CTRL-S but with the aerosol-radiation interaction  
373 turned off. The difference of results between NoRA-S and CLEAN-S (NoRA-S minus  
374 CLEAN-S) is interpreted as the impacts of aerosol-cloud interaction, while the difference of  
375 results between CTRL-S and NoRA-S (CTRL-S minus NoRA-S) is interpreted as the impacts  
376 of aerosol-radiation interactions. Figure 10 shows the spatial distribution the impacts of  
377 aerosol-cloud and aerosol-radiation interactions on (a, d) tropospheric temperature averaged  
378 below 500 hPa, (b, e) surface pressure, (c, f) precipitation and moisture transport. The aerosol-  
379 cloud interaction reduces significantly the lower tropospheric temperature (Fig. 10a) over a  
380 large area of South China (to the south of 32°N) due to its increasing of cloud amounts (Fig.  
381 S6a in the supporting material) over this area, which results in an increase of surface pressure  
382 in this area (Fig. 10b). Similarly, aerosol-cloud interaction also increases cloud amounts over  
383 Northeast China and its adjacent ocean (Fig. S6a) and thus reduces the lower tropospheric  
384 temperature and increases the surface pressure over the area. The surface pressure over the  
385 Yellow River Basin is reduced slightly by aerosol-cloud interaction due to the reduction of  
386 cloud amounts (Fig. S6a) and the increase of lower tropospheric temperature. The difference  
387 between NoRA-S and CLEAN-S over Northwest China is due to the dust-radiation interaction  
388 that is included in CLEAN-S but not in NoRA-S. The analysis of this study focuses on the  
389 impacts of anthropogenic aerosol. The combined effect of two anti-cyclone anomalies due to  
390 the two positive pressure anomalies at the lower troposphere results in the southward wind  
391 anomalies over the ocean and the northward wind anomalies over North China, while the  
392 changes of circulations in other areas of China is negligible.

393 The primary impacts of aerosol-radiation interaction on lower-atmospheric temperature  
394 are the positive temperature anomalies over the Yellow Ocean and over central China and the  
395 negative temperature anomalies over the Yellow River Basin and Southwest China, which is  
396 the combined effects from the aerosol cooling at the surface and heating in the atmosphere and  
397 also the adjustment of cloud distributions (Fig. S6b and Fig. S7). The two positive temperature



398 anomaly centers lead to two negative pressure anomaly centers and thus a large cyclone  
399 circulation anomaly over the continent of East China. Therefore, it can be noted that the  
400 influence of aerosol-cloud and aerosol-radiation interactions on monsoonal circulations are  
401 counteracted over the ocean and over northern China, which results in relatively small changes  
402 of monsoonal circulation over the ocean and over northern China (Fig. 8). The overall aerosol  
403 impact is shown as the weakening of the monsoonal circulation over the continent of central  
404 and southern China (Fig. 8), which is mainly contributed by the aerosol-radiation interaction.

405 Figure 11 shows the latitude-pressure cross-section of aerosol-induced difference  
406 (CTRL-CLEAN) of temperature and wind averaged between 105°E and 122°E for June and  
407 July of 2017 from the small domain simulation. It can be seen that the pattern of precipitation  
408 change corresponds well to the changes of wind circulation. The weakening of monsoonal  
409 southwesterlies result in a sinking airflow anomaly around 28°N and the compensating upward  
410 anomaly around 24°N in the south of China, and also a downdraft around 35°N and an updraft  
411 around 40°N in north China. These two sinking airflows corresponds to the reduced  
412 precipitation between 25°N and 30°N and between 32°N and 40°N, respectively (Fig. 8), while  
413 these updrafts correspond to the increasing precipitation between 22°N and 25°N and between  
414 32°N and 40°N. There is also weak upward compensating airflow around 30°N, leading to the  
415 slight increase of precipitation in the area (Fig. 8). It is noteworthy that aerosols lead to an  
416 abnormal cooling center around 33°N between 400 hPa to 200 hPa. This is mainly because of  
417 less solar radiation entering the atmosphere due to aerosol-radiation and aerosol-cloud  
418 interactions, and also weaker monsoonal airflow that leads to less release of latent heat from  
419 cloud and precipitation (Fig. S8 in the supporting material). This cooling anomaly center also  
420 strengthens the downdraft anomalies on its both sides, further weakening the monsoonal  
421 circulation.

422 In order to explore the sensitivity of aerosol impacts to domain size, similar as Fig. 8,  
423 Figure 12 shows the results from the large domain simulations. One consistent signal between  
424 the simulations with different domain sizes is that aerosols weaken the southwesterlies flow  
425 and reduce the moisture transport over the continent of Central and South China. The difference  
426 is that this weakening is not only over the inland of China but also extending to over the South  
427 China Ocean. The weakening of monsoon airflow is broader with the increasing domain size,  
428 which may be due to its weaker monsoon airflow (Fig. 3) and less constraint from the lateral  
429 boundaries in the large domain simulation. Another consistent signal between the two sets of  
430 simulations with different domain sizes is that aerosol induces a similar “+--+” pattern of  
431 precipitation changes over the domain, except that the areas with precipitation reduction



432 become broader. This leads to the precipitation reduction over almost the entire region between  
433 20°N~40°N over the continent of China except the area around 30°N with increasing  
434 precipitation. The increases of precipitation on the two sides of precipitation reduction area  
435 shift southward to the South China ocean and northward to the north of 40°N, respectively.

436 Similar as the small domain simulation, the weakening of monsoonal airflow in the  
437 large domain simulation is also due to the abnormal positive lower-level pressure that is caused  
438 by the lower atmosphere cooling (Fig. 13), which can also be explained by the effects of  
439 aerosol-radiation and aerosol-cloud interactions (Fig. S9 and Fig. S10 in the supporting  
440 material). However, compared with the small domain simulation (Fig. 9), the cooling anomaly  
441 of lower-tropospheric temperature and thus the positive anomaly of lower-level pressure cover  
442 a broader area from the large domain simulation. The two aerosol-induced cooling centers over  
443 the continent of China lead to two positive lower-level pressure anomaly that results in a large  
444 anti-cycle circulation anomaly (Fig. 12), which weakens the monsoonal southwesterly airflow  
445 over South China and the South China Ocean and also slightly enhances the southwesterly over  
446 West China. Again, the pattern of precipitation change corresponds well to the changes of wind  
447 circulation (Fig. 14). With larger domain size, aerosols lead to a broader area (between  
448 20°N~40°N) of abnormal cooling in the troposphere up to 200 hPa. The single cooling center  
449 in the small domain simulation is split into two centers, one around 30°N at 250 hPa and  
450 another around 36°N at 700 hPa. The weakening of the background circulation and broader  
451 cooling area lead to the broader sinking airflows over the region, which results in the broader  
452 area of reduced precipitation compared with the small domain simulation (Fig. 8 and Fig. 12).  
453 The increasing precipitation around 30°N is also resulted from the compensating updrafts  
454 around 30°N.

455

#### 456 **4. Summary and Discussion**

457 Due to the importance of domain size on regional modeling results and few studies  
458 examining the sensitivities of regional modeling results of aerosol impacts to domain size, this  
459 study applies the WRF-Chem model to simulate the anthropogenic aerosol impacts on East  
460 Asian summer monsoon circulation and precipitation, focusing on the modeling sensitivities to  
461 regional domain size. The impacts of domain size on meteorological fields, aerosol  
462 characteristics, and aerosol impacts are investigated.

463 First of all, the domain size has a great influence on the simulated meteorological fields.  
464 From the small domain simulation, the circulation and precipitation are in good agreement with



465 the reanalysis data and observations. The large domain simulation produces weaker East Asian  
466 summer monsoon system shifting southward, which results in the precipitation decrease in  
467 southern China and increase in the adjacent ocean. The changes of circulation and precipitation  
468 also lead to the increase of aerosol mass loading in southern China and the decrease in northern  
469 China in the large domain simulation. The deviation of atmospheric fields particularly the  
470 circulation between the simulations with different domains is partly due to their different  
471 constraint from lateral boundary conditions. With less constraint of the boundary forcing from  
472 the reanalysis data, the large domain simulation may produce negative bias in precipitation  
473 over the Yangtze River Basin and positive bias in water vapor transport over the South China  
474 Ocean as previous studies. The uncertainties in moisture transport prescribed in the lateral  
475 boundaries from the reanalysis over a larger domain may also contribute to the biases (e.g.,  
476 Wang and Yang, 2008; Huang and Gao, 2018). With the larger domain, the simulation includes  
477 larger area of ocean. Without considering the online interaction between the atmosphere and  
478 the ocean (i.e., with prescribed SST from the reanalysis), the artificial positive feedback  
479 between precipitation and surface latent heat flux may overestimate the precipitation over the  
480 subtropical Western North Pacific (WNP) and inhibit the westward expansion of the WNP  
481 subtropical high (e.g., Cha and Lee, 2009; Lee and Cha, 2020).

482 In terms of the climatic impacts of anthropogenic aerosols on East Asian summer  
483 monsoon, as shown in the schematic plot (Fig. 15), aerosols induce the cooling of lower  
484 troposphere over the continent through aerosol-radiation and aerosol-cloud interactions, which  
485 leads to an increase of regional pressure at lower atmosphere. The regional positive pressure  
486 anomalies result in the anti-cyclone circulation anomalies and thus weakens the summer  
487 monsoonal northeastward moisture transport, which is consistent with previous studies (e.g.,  
488 Y. Q. Jiang et al., 2013; Song et al., 2014; T. J. Wang et al., 2015; Xie et al., 2016). The  
489 weakening of monsoonal circulation leads to several sinking airflows and compensating  
490 updrafts that correspond well to the regions with the decrease and increase of precipitation,  
491 respectively, showing a spatial pattern of “+--+” for precipitation change. The difference in  
492 the aerosol impacts from the numerical experiments with different domain sizes is mainly  
493 determined by their simulated different strength and area extent of the aerosol-induced lower-  
494 tropospheric negative temperature anomalies. Compared with the smaller-domain simulation,  
495 the larger-domain simulation with weaker monsoonal circulation generates a broader area with  
496 negative temperature and positive pressure anomalies at the lower troposphere, which results  
497 in broader sinking airflows and thus broader areas of precipitation reduction over the continent  
498 of China. This could lead to the opposite signals of precipitation change due to aerosols over



499 China, for example, over Southeast China, the increase and decrease of precipitation from the  
500 smaller-domain and larger-domain simulations, respectively. The consistent signal of aerosol  
501 impacts between the simulations with different domain sizes is the increasing precipitation  
502 around 30°N that is resulted from the compensating updraft over the region.

503 Although the modeling results of aerosol impacts in this study may have some  
504 uncertainties associated with physical and chemical processes, emissions, and simulation  
505 horizontal resolutions, it highlights the impacts of simulation domain size on regional modeling  
506 aerosol impacts on monsoonal circulation and precipitation, which may not be limited to the  
507 region of East Asia. Uncertainties of modeling aerosol climatic impacts are often investigated  
508 focusing on aerosol characteristics such as their distributions and properties. This study adds  
509 another complexity (impact of domain size) on regional modeling of aerosol climatic impacts.  
510 More specifically, although larger-domain simulation may better allow feedbacks of aerosol  
511 impacts on weather and climate systems without strong lateral boundary constraint (e.g., Seth  
512 and Giorgi, 1998; Leduc and Laprise, 2009), it may produce biased meteorological fields  
513 compared to smaller-domain simulation, which can significantly influence the modeling results  
514 of aerosol impacts. It may be the key to simulate reasonable/less biased meteorological fields  
515 with larger regional domain or global domain in order to model robust aerosol climatic impacts.  
516 More generally, this study also highlights the impacts of background meteorological fields  
517 (without aerosol effect) on simulated aerosol impacts. Proper modeling of background  
518 meteorological fields is one of the keys to simulate robust aerosol climatic impacts. The model  
519 inter-comparison study of aerosol climatic impacts should also focus on the diversity of  
520 simulated background meteorological fields besides aerosol characteristics.

521

522

### 523 **Code and data availability**

524 The release version of WRF-Chem can be downloaded from  
525 [http://www2.mmm.ucar.edu/wrf/users/download/get\\_source.html](http://www2.mmm.ucar.edu/wrf/users/download/get_source.html). The code of updated  
526 USTC version of WRF-Chem is available at <https://doi.org/10.5281/zenodo.4663508> or  
527 contact [chunzhao@ustc.edu.cn](mailto:chunzhao@ustc.edu.cn). The dataset from the European Centre for Medium-Range  
528 Weather Forecasts (ECMWF) Reanalysis (ERA5) can be downloaded from  
529 <https://rda.ucar.edu/datasets/ds633.1/> (last access: Aug 2021). The CMORPH data can be  
530 downloaded from [https://ftp.cpc.ncep.noaa.gov/precip/CMORPH\\_V1.0/CRT/0.25deg-](https://ftp.cpc.ncep.noaa.gov/precip/CMORPH_V1.0/CRT/0.25deg-DLY_00Z/2017/)  
531 [DLY\\_00Z/2017/](https://ftp.cpc.ncep.noaa.gov/precip/CMORPH_V1.0/CRT/0.25deg-DLY_00Z/2017/) (last access: Aug 2021).





532

533 **Author contributions**

534 Xiaodong Wang and Chun Zhao designed the experiments, conducted and analyzed the  
535 simulations. All authors contributed to the discussion and final version of the paper.

536

537 **Acknowledgements**

538 This research was supported by the National Natural Science Foundation of China  
539 (42061134009, 41775146, 91837310), the USTC Research Funds of the Double First-Class  
540 Initiative (YD2080002007), Fundamental Research Funds for the Central Universities  
541 (WK2080000101), and the Strategic Priority Research Program of Chinese Academy of  
542 Sciences (XDB41000000). The study used the computing resources from the High-  
543 Performance Computing Center of University of Science and Technology of China (USTC)  
544 and the TH-2 of National Supercomputer Center in Guangzhou (NSCC-GZ).

545

546



547 **Reference**

- 548 Ackerman, A. S., Toon, O. B., Stevens, D. E., Heymsfield, A. J., Ramanathan, V., & Welton,  
549 E. J. (2000). Reduction of tropical cloudiness by soot. *Science*, **288**(5468), 1042-1047.  
550 <https://doi.org/10.1126/science.288.5468.1042>
- 551 Albrecht, B. A. (1989). Aerosols, Cloud Microphysics, and Fractional Cloudiness. *Science*,  
552 **245**(4923), 1227-1230. <https://doi.org/10.1126/science.245.4923.1227>
- 553 An, Z. S., Wu, G. X., Li, J. P., Sun, Y. B., Liu, Y. M., Zhou, W. J., et al. (2015). Global  
554 Monsoon Dynamics and Climate Change. *Annual Review of Earth and Planetary*  
555 *Sciences*, **43**, 29-77. <https://doi.org/10.1146/annurev-earth-060313-054623>
- 556 An, Z. S., Huang, R. J., Zhang, R. Y., Tie, X. X., Li, G. H., Cao, J. J., et al. (2019). Severe haze  
557 in northern China: A synergy of anthropogenic emissions and atmospheric processes.  
558 *Proceedings of the National Academy of Sciences of the United States of America*,  
559 **116**(18), 8657-8666. <https://doi.org/10.1073/pnas.1900125116>
- 560 Bhaskaran, B., Ramachandran, A., Jones, R., & Moufouma-Okia, W. (2012). Regional climate  
561 model applications on sub-regional scales over the Indian monsoon region: The role of  
562 domain size on downscaling uncertainty. *Journal of Geophysical Research-*  
563 *Atmospheres*, **117**. <https://doi.org/10.1029/2012jd017956>
- 564 Binkowski, F. S., & Shankar, U. (1995). The Regional Particulate Matter Model .1. Model  
565 description and preliminary results. *Journal of Geophysical Research-Atmospheres*,  
566 **100**(D12), 26191-26209. <https://doi.org/10.1029/95jd02093>
- 567 Carvalho, D., Rocha, A., Gomez-Gesteira, M., & Santos, C. S. (2014). WRF wind simulation  
568 and wind energy production estimates forced by different reanalyses: Comparison with  
569 observed data for Portugal. *Applied Energy*, **117**, 116-126.  
570 <https://doi.org/10.1016/j.apenergy.2013.12.001>
- 571 Cha, D. H., & Lee, D. K. (2009). Reduction of systematic errors in regional climate simulations  
572 of the summer monsoon over East Asia and the western North Pacific by applying the  
573 spectral nudging technique. *Journal of Geophysical Research-Atmospheres*, **114**.  
574 <https://doi.org/10.1029/2008jd011176>
- 575 Chan, C. K., & Yao, X. (2008). Air pollution in mega cities in China. *Atmospheric Environment*,  
576 **42**(1), 1-42. <https://doi.org/10.1016/j.atmosenv.2007.09.003>
- 577 Chapman, E. G., Gustafson, W. I., Easter, R. C., Barnard, J. C., Ghan, S. J., Pekour, M. S., &  
578 Fast, J. D. (2009). Coupling aerosol-cloud-radiative processes in the WRF-Chem model:



- 579 Investigating the radiative impact of elevated point sources. *Atmospheric Chemistry*  
580 *and Physics*, **9**(3), 945-964. <https://doi.org/10.5194/acp-9-945-2009>
- 581 Chen, S. Y., Zhao, C., Qian, Y., Leung, L. R., Huang, J. P., Huang, Z. W., et al. (2014).  
582 Regional modeling of dust mass balance and radiative forcing over East Asia using  
583 WRF-Chem. *Aeolian Research*, **15**, 15-30.  
584 <https://doi.org/10.1016/j.aeolia.2014.02.001>
- 585 Chen, J. P., Chen, I. J., & Tsai, I. C. (2016). Dynamic Feedback of Aerosol Effects on the East  
586 Asian Summer Monsoon. *Journal of Climate*, **29**(17), 6137-6149.  
587 <https://doi.org/10.1175/Jcli-D-15-0758.1>
- 588 Colin, J., Deque, M., Radu, R., & Somot, S. (2010). Sensitivity study of heavy precipitation in  
589 Limited Area Model climate simulations: influence of the size of the domain and the  
590 use of the spectral nudging technique. *Tellus Series a-Dynamic Meteorology and*  
591 *Oceanography*, **62**(5), 591-604. <https://doi.org/10.1111/j.1600-0870.2010.00467.x>
- 592 Cowan, T., & Cai, W. (2011). The impact of Asian and non-Asian anthropogenic aerosols on  
593 20th century Asian summer monsoon. *Geophysical Research Letters*, **38**.  
594 <https://doi.org/10.1029/2011gl047268>
- 595 Davies, T. (2014). Lateral boundary conditions for limited area models. *Quarterly Journal of*  
596 *the Royal Meteorological Society*, **140**(678), 185-196. <https://doi.org/10.1002/qj.2127>
- 597 Dentener, F., Kinne, S., Bond, T., Boucher, O., Cofala, J., Generoso, S., et al. (2006). Emissions  
598 of primary aerosol and precursor gases in the years 2000 and 1750 prescribed data-sets  
599 for AeroCom. *Atmospheric Chemistry and Physics*, **6**, 4321-4344.  
600 <https://doi.org/10.5194/acp-6-4321-2006>
- 601 Diner, D. J., Beckert, J. C., Reilly, T. H., Bruegge, C. J., Conel, J. E., Kahn, R. A., et al. (1998).  
602 Multi-angle Imaging SpectroRadiometer (MISR) - Instrument description and  
603 experiment overview. *Ieee Transactions on Geoscience and Remote Sensing*, **36**(4),  
604 1072-1087. <https://doi.org/10.1109/36.700992>
- 605 Diner, D. J., Abdou, W. A., Bruegge, C. J., Conel, J. E., Crean, K. A., Gaitley, B. J., et al.  
606 (2001). MISR aerosol optical depth retrievals over southern Africa during the SAFARI-  
607 2000 dry season campaign. *Geophysical Research Letters*, **28**(16), 3127-3130.  
608 <https://doi.org/10.1029/2001gl013188>
- 609 Ding, Y. H., & Chan, J. C. L. (2005). The East Asian summer monsoon: an overview.  
610 *Meteorology and Atmospheric Physics*, **89**(1-4), 117-142.  
611 <https://doi.org/10.1007/s00703-005-0125-z>



- 612 Ding, Y. H. (2007). The variability of the Asian summer monsoon. *Journal of the*  
613 *Meteorological Society of Japan*, **85b**, 21-54. <https://doi.org/10.2151/jmsj.85B.21>
- 614 Ding, Y. H., Wang, Z. Y., & Sun, Y. (2008). Inter-decadal variation of the summer  
615 precipitation in East China and its association with decreasing Asian summer monsoon.  
616 Part I: Observed evidences. *International Journal of Climatology*, **28**(9), 1139-1161.  
617 <https://doi.org/10.1002/joc.1615>
- 618 Ding, Y. H., Sun, Y., Wang, Z. Y., Zhu, Y. X., & Song, Y. F. (2009). Inter-decadal variation  
619 of the summer precipitation in China and its association with decreasing Asian summer  
620 monsoon Part II: Possible causes. *International Journal of Climatology*, **29**(13), 1926-  
621 1944. <https://doi.org/10.1002/joc.1759>
- 622 Ding, Y., Sun, Y., Liu, Y., Si, D., Wang, Z., Zhu, Y., et al. (2013). Interdecadal and Interannual  
623 Variabilities of the Asian Summer Monsoon and Its Projection of Future Change.  
624 *Chinese Journal of Atmospheric Sciences*, **37**(2), 253-280.
- 625 Ding, A. J., Fu, C. B., Yang, X. Q., Sun, J. N., Petaja, T., Kerminen, V. M., et al. (2013).  
626 Intense atmospheric pollution modifies weather: a case of mixed biomass burning with  
627 fossil fuel combustion pollution in eastern China. *Atmospheric Chemistry and Physics*,  
628 **13**(20), 10545-10554. <https://doi.org/10.5194/acp-13-10545-2013>
- 629 Dong, B. W., Wilcox, L. J., Highwood, E. J., & Sutton, R. T. (2019). Impacts of recent decadal  
630 changes in Asian aerosols on the East Asian summer monsoon: roles of aerosol-  
631 radiation and aerosol-cloud interactions. *Climate Dynamics*, **53**(5-6), 3235-3256.  
632 <https://doi.org/10.1007/s00382-019-04698-0>
- 633 Du, Q. Y., Zhao, C., Zhang, M. S., Dong, X., Chen, Y., Liu, Z., et al. (2020). Modeling diurnal  
634 variation of surface PM<sub>2.5</sub> concentrations over East China with WRF-Chem: impacts  
635 from boundary-layer mixing and anthropogenic emission. *Atmospheric Chemistry and*  
636 *Physics*, **20**(5), 2839-2863. <https://doi.org/10.5194/acp-20-2839-2020>
- 637 Easter, R. C., Ghan, S. J., Zhang, Y., Saylor, R. D., Chapman, E. G., Laulainen, N. S., et al.  
638 (2004). MIRAGE: Model description and evaluation of aerosols and trace gases.  
639 *Journal of Geophysical Research-Atmospheres*, **109**(D20).  
640 <https://doi.org/10.1029/2004jd004571>
- 641 European Centre for Medium-Range Weather Forecasts (2019), ERA5 Reanalysis (0.25  
642 Degree Latitude-Longitude Grid), <https://doi.org/10.5065/BH6N-5N20>, Research Data  
643 Archive at the National Center for Atmospheric Research, Computational and  
644 Information Systems Laboratory, Boulder, Colo. (Updated monthly.) Accessed 27 Dec  
645 2020.



- 646 Fan, J. W., Rosenfeld, D., Ding, Y. N., Leung, L. R., & Li, Z. Q. (2012). Potential aerosol  
647 indirect effects on atmospheric circulation and radiative forcing through deep  
648 convection. *Geophysical Research Letters*, **39**. <https://doi.org/10.1029/2012gl051851>
- 649 Fan, J. W., Leung, L. R., Rosenfeld, D., Chen, Q., Li, Z. Q., Zhang, J. Q., & Yan, H. R. (201  
650 3). Microphysical effects determine macrophysical response for aerosol impacts on de  
651 ep convective clouds. *Proceedings of the National Academy of Sciences of the United*  
652 *States of America*, **110**(48), E4581-E4590. <https://doi.org/10.1073/pnas.1316830110>
- 653 Fan, J. W., Rosenfeld, D., Yang, Y., Zhao, C., Leung, L. R., & Li, Z. Q. (2015). Substantial c  
654 ontribution of anthropogenic air pollution to catastrophic floods in Southwest China.  
655 *Geophysical Research Letters*, **42**(14), 6066-6075. <https://doi.org/10.1002/2015gl064>  
656 479
- 657 Fan, J. W., Wang, Y., Rosenfeld, D., & Liu, X. H. (2016). Review of Aerosol-Cloud Interacti  
658 ons: Mechanisms, Significance, and Challenges. *Journal of the Atmospheric Sciences*,  
659 **73**(11), 4221-4252. <https://doi.org/10.1175/Jas-D-16-0037.1>
- 660 Fan, J. W., Rosenfeld, D., Zhang, Y. W., Giangrande, S. E., Li, Z. Q., Machado, L. A. T., et a  
661 l. (2018). Substantial convection and precipitation enhancements by ultrafine aerosol  
662 particles. *Science*, **359**(6374), 411-418. <https://doi.org/10.1126/science.aan8461>
- 663 Fast, J. D., Gustafson, W. I., Easter, R. C., Zaveri, R. A., Barnard, J. C., Chapman, E. G., et a  
664 l. (2006). Evolution of ozone, particulates, and aerosol direct radiative forcing in the v  
665 icinity of Houston using a fully coupled meteorology-chemistry-aerosol model. *Journ*  
666 *al of Geophysical Research-Atmospheres*, **111**(D21). <https://doi.org/10.1029/2005jd00>  
667 6721
- 668 Gao, Y., Zhao, C., Liu, X. H., Zhang, M. G., & Leung, L. R. (2014). WRF-Chem simulations  
669 of aerosols and anthropogenic aerosol radiative forcing in East Asia. *Atmospheric Env*  
670 *ironment*, **92**, 250-266. <https://doi.org/10.1016/j.atmosenv.2014.04.038>
- 671 Ginoux, P., Chin, M., Tegen, I., Prospero, J. M., Holben, B., Dubovik, O., & Lin, S. J. (2001).  
672 Sources and distributions of dust aerosols simulated with the GOCART model. *Journ*  
673 *al of Geophysical Research-Atmospheres*, **106**(D17), 20255-20273. [https://doi.org/10.](https://doi.org/10.1029/2000jd000053)  
674 [1029/2000jd000053](https://doi.org/10.1029/2000jd000053)
- 675 Giorgi, F. (2019). Thirty Years of Regional Climate Modeling: Where Are We and Where Ar  
676 e We Going next? *Journal of Geophysical Research-Atmospheres*, **124**(11), 5696-572  
677 3. <https://doi.org/10.1029/2018jd030094>



- 678 Grell, G. A., Peckham, S. E., Schmitz, R., McKeen, S. A., Frost, G., Skamarock, W. C., & Ed  
679 er, B. (2005). Fully coupled "online" chemistry within the WRF model. *Atmospheric*  
680 *Environment*, **39**(37), 6957-6975. <https://doi.org/10.1016/j.atmosenv.2005.04.027>
- 681 Guo, L., Highwood, E. J., Shaffrey, L. C., & Turner, A. G. (2013). The effect of regional chan  
682 ges in anthropogenic aerosols on rainfall of the East Asian Summer Monsoon. *Atmosp*  
683 *heric Chemistry and Physics*, **13**(3), 1521-1534. [https://doi.org/10.5194/acp-13-1521-](https://doi.org/10.5194/acp-13-1521-2013)  
684 2013
- 685 Hu, Z. Y., Zhao, C., Huang, J. P., Leung, L. R., Qian, Y., Yu, H. B., et al. (2016). Trans-Pacif  
686 ic transport and evolution of aerosols: evaluation of quasi-global WRF-Chem simulati  
687 on with multiple observations. *Geoscientific Model Development*, **9**(5), 1725-1746. <https://doi.org/10.5194/gmd-9-1725-2016>
- 689 Hu, Z. Y., Huang, J. P., Zhao, C., Bi, J. R., Jin, Q. J., Qian, Y., et al. (2019). Modeling the co  
690 ntributions of Northern Hemisphere dust sources to dust outflow from East Asia. *Atmo*  
691 *spheric Environment*, **202**, 234-243. <https://doi.org/10.1016/j.atmosenv.2019.01.022>
- 692 Huang, D. L., & Gao, S. B. (2018). Impact of different reanalysis data on WRF dynamical do  
693 wnscales over China. *Atmospheric Research*, **200**, 25-35. [https://doi.org/10.1016/j.at](https://doi.org/10.1016/j.atmosres.2017.09.017)  
694 mosres.2017.09.017
- 695 Huang, R., & Chen, J. (2010). Characteristics of the Summertime Water Vapor Transports ov  
696 er the Eastern Part of China and Those over the Western Part of China and Their Diffe  
697 rence. *Chinese Journal of Atmospheric Sciences*, **34**(6), 1035-1046.
- 698 Huang, X., Ding, A. J., Liu, L. X., Liu, Q., Ding, K., Niu, X. R., et al. (2016). Effects of aeros  
699 ol-radiation interaction on precipitation during biomass-burning season in East China.  
700 *Atmospheric Chemistry and Physics*, **16**(15), 10063-10082. [https://doi.org/10.5194/ac](https://doi.org/10.5194/acp-16-10063-2016)  
701 p-16-10063-2016
- 702 Iacono, M. J., Mlawer, E. J., Clough, S. A., & Morcrette, J. J. (2000). Impact of an improved l  
703 ongwave radiation model, RRTM, on the energy budget and thermodynamic propertie  
704 s of the NCAR community climate model, CCM3. *Journal of Geophysical Research-*  
705 *Atmospheres*, **105**(D11), 14873-14890. <https://doi.org/10.1029/2000jd900091>
- 706 Iacono, M. J., Delamere, J. S., Mlawer, E. J., Shephard, M. W., Clough, S. A., & Collins, W.  
707 D. (2008). Radiative forcing by long-lived greenhouse gases: Calculations with the A  
708 ER radiative transfer models. *Journal of Geophysical Research-Atmospheres*, **113**(D1  
709 3). <https://doi.org/10.1029/2008jd009944>
- 710 IPCC, 2013: *Climate Change 2013: The Physical Science Basis. Contribution of Working*  
711 *Group I to the Fifth Assessment Report of the Intergovernmental Panel on Climate*



- 712            *Change* [Stocker, T.F., D. Qin, G.-K. Plattner, M. Tignor, S.K. Allen, J. Boschung, A.  
713            Nauels, Y. Xia, V. Bex and P.M. Midgley (eds.)]. Cambridge University Press,  
714            Cambridge, United Kingdom and New York, NY, USA, 1535 pp.
- 715            Janssens-Maenhout, G., Crippa, M., Guizzardi, D., Dentener, F., Muntean, M., Pouliot, G., et  
716            al. (2015). HTAP\_v2.2: a mosaic of regional and global emission grid maps for 2008  
717            and 2010 to study hemispheric transport of air pollution. *Atmospheric Chemistry and*  
718            *Physics*, **15**(19), 11411-11432. <https://doi.org/10.5194/acp-15-11411-2015>
- 719            Jiang, Y. Q., Liu, X. H., Yang, X. Q., & Wang, M. H. (2013). A numerical study of the effect  
720            of different aerosol types on East Asian summer clouds and precipitation. *Atmospheric*  
721            *Environment*, **70**, 51-63. <https://doi.org/10.1016/j.atmosenv.2012.12.039>
- 722            Jiang, Z. H., Huo, F., Ma, H. Y., Song, J., & Dai, A. G. (2017). Impact of Chinese Urbanization  
723            and Aerosol Emissions on the East Asian Summer Monsoon. *Journal of Climate*, **30**(3),  
724            1019-1039. <https://doi.org/10.1175/Jcli-D-15-0593.1>
- 725            Joyce, R. J., Janowiak, J. E., Arkin, P. A., & Xie, P. P. (2004). CMORPH: A method that  
726            produces global precipitation estimates from passive microwave and infrared data at  
727            high spatial and temporal resolution. *Journal of Hydrometeorology*, **5**(3), 487-503.  
728            [https://doi.org/10.1175/1525-7541\(2004\)005<0487:Camtpg>2.0.Co;2](https://doi.org/10.1175/1525-7541(2004)005<0487:Camtpg>2.0.Co;2)
- 729            Kain, J. S. (2004). The Kain-Fritsch convective parameterization: An update. *Journal of*  
730            *Applied Meteorology*, **43**(1), 170-181. [https://doi.org/10.1175/1520-0450\(2004\)043<0170:Tkcpan>2.0.Co;2](https://doi.org/10.1175/1520-0450(2004)043<0170:Tkcpan>2.0.Co;2)
- 732            Kim, M. J., Yeh, S. W., & Park, R. J. (2016). Effects of sulfate aerosol forcing on East Asian  
733            summer monsoon for 1985-2010. *Geophysical Research Letters*, **43**(3), 1364-1372.  
734            <https://doi.org/10.1002/2015gl067124>
- 735            Kim, M. K., Lau, W. K. M., Kim, K. M., & Lee, W. S. (2007). A GCM study of effects of  
736            radiative forcing of sulfate aerosol on large scale circulation and rainfall in East Asia  
737            during boreal spring. *Geophysical Research Letters*, **34**(24).  
738            <https://doi.org/10.1029/2007gl031683>
- 739            Kok, J. F. (2011). A scaling theory for the size distribution of emitted dust aerosols suggests  
740            climate models underestimate the size of the global dust cycle. *Proceedings of the*  
741            *National Academy of Sciences of the United States of America*, **108**(3), 1016-1021.  
742            <https://doi.org/10.1073/pnas.1014798108>
- 743            Kuniyal, J. C., & Guleria, R. P. (2019). The current state of aerosol-radiation interactions: A  
744            mini review. *Journal of Aerosol Science*, **130**, 45-54.  
745            <https://doi.org/10.1016/j.jaerosci.2018.12.010>



- 746 Leduc, M., & Laprise, R. (2009). Regional climate model sensitivity to domain size. *Climate*  
747 *Dynamics*, **32**(6), 833-854. <https://doi.org/10.1007/s00382-008-0400-z>
- 748 Leduc, M., Laprise, R., Moretti-Poisson, M., & Morin, J. P. (2011). Sensitivity to domain size  
749 of mid-latitude summer simulations with a regional climate model. *Climate Dynamics*,  
750 **37**(1-2), 343-356. <https://doi.org/10.1007/s00382-011-1008-2>
- 751 Lee, D. K., & Cha, D. H. (2020). Regional climate modeling for Asia. *Geoscience Letters*, **7**(1).  
752 <https://doi.org/10.1186/s40562-020-00162-8>
- 753 Li, M., Liu, H., Geng, G. N., Hong, C. P., Liu, F., Song, Y., et al. (2017). Anthropogenic  
754 emission inventories in China: a review. *National Science Review*, **4**(6), 834-866.  
755 <https://doi.org/10.1093/nsr/nwx150>
- 756 Li, H. M., Dai, A. G., Zhou, T. J., & Lu, J. (2010). Responses of East Asian summer monsoon  
757 to historical SST and atmospheric forcing during 1950-2000. *Climate Dynamics*, **34**(4),  
758 501-514. <https://doi.org/10.1007/s00382-008-0482-7>
- 759 Li, X. Q., Ting, M. F., Li, C. H., & Henderson, N. (2015). Mechanisms of Asian Summer  
760 Monsoon Changes in Response to Anthropogenic Forcing in CMIP5 Models. *Journal*  
761 *of Climate*, **28**(10), 4107-4125. <https://doi.org/10.1175/Jcli-D-14-00559.1>
- 762 Li, X. Q., Ting, M. F., & Lee, D. E. (2018). Fast Adjustments of the Asian Summer Monsoon  
763 to Anthropogenic Aerosols. *Geophysical Research Letters*, **45**(2), 1001-1010.  
764 <https://doi.org/10.1002/2017gl076667>
- 765 Li, Z. Q., Lee, K. H., Wang, Y. S., Xin, J. Y., & Hao, W. M. (2010). First observation-based  
766 estimates of cloud-free aerosol radiative forcing across China. *Journal of Geophysical*  
767 *Research-Atmospheres*, **115**. <https://doi.org/10.1029/2009jd013306>
- 768 Li, Z. Q., Lau, W. K. M., Ramanathan, V., Wu, G., Ding, Y., Manoj, M. G., et al. (2016).  
769 Aerosol and monsoon climate interactions over Asia. *Reviews of Geophysics*, **54**(4),  
770 866-929. <https://doi.org/10.1002/2015rg000500>
- 771 Li, Z. Q., Wang, Y., Guo, J. P., Zhao, C. F., Cribb, M., Dong, X. Q., et al. (2019). East Asian  
772 Study of Tropospheric Aerosols and their Impact on Regional Clouds, Precipitation,  
773 and Climate (EAST-AIR(CPC)). *Journal of Geophysical Research-Atmospheres*,  
774 **124**(23), 13026-13054. <https://doi.org/10.1029/2019jd030758>
- 775 Liu, H. Y., Jacob, D. J., Bey, I., & Yantosca, R. M. (2001). Constraints from Pb-210 and Be-7  
776 on wet deposition and transport in a global three-dimensional chemical tracer model  
777 driven by assimilated meteorological fields. *Journal of Geophysical Research-*  
778 *Atmospheres*, **106**(D11), 12109-12128. <https://doi.org/10.1029/2000jd900839>





- 779 Liu, J. Z., Li, J., & Li, W. F. (2016). Temporal Patterns in Fine Particulate Matter Time Series  
780 in Beijing: A Calendar View. *Scientific Reports*, **6**. <https://doi.org/10.1038/srep32221>
- 781 Luo, Y. X., Zheng, X. B., Zhao, T. L., & Chen, J. (2014). A climatology of aerosol optical  
782 depth over China from recent 10 years of MODIS remote sensing data. *International*  
783 *Journal of Climatology*, **34**(3), 863-870. <https://doi.org/10.1002/joc.3728>
- 784 Morrison, H., Thompson, G., & Tatarskii, V. (2009). Impact of Cloud Microphysics on the  
785 Development of Trailing Stratiform Precipitation in a Simulated Squall Line:  
786 Comparison of One- and Two-Moment Schemes. *Monthly Weather Review*, **137**(3),  
787 991-1007. <https://doi.org/10.1175/2008mwr2556.1>
- 788 Mlawer, E. J., Taubman, S. J., Brown, P. D., Iacono, M. J., & Clough, S. A. (1997). Radiative  
789 transfer for inhomogeneous atmospheres: RRTM, a validated correlated-k model for  
790 the longwave. *Journal of Geophysical Research-Atmospheres*, **102**(D14), 16663-16682.  
791 <https://doi.org/10.1029/97jd00237>
- 792 Myhre, G., D. Shindell, F.-M. Bréon, W. Collins, J. Fuglestedt, J. Huang, D. Koch, J.-F.  
793 Lamarque, D. Lee, B. Mendoza, T. Nakajima, A. Robock, G. Stephens, T. Takemura  
794 and H. Zhang, 2013: Anthropogenic and Natural Radiative Forcing. In: Climate Change  
795 2013: The Physical Science Basis. Contribution of Working Group I to the Fifth  
796 Assessment Report of the Intergovernmental Panel on Climate Change [Stocker, T.F.,  
797 D. Qin, G.-K. Plattner, M. Tignor, S.K. Allen, J. Boschung, A. Nauels, Y. Xia, V. Bex  
798 and P.M. Midgley (eds.)]. Cambridge University Press, Cambridge, United Kingdom  
799 and New York, NY, USA.
- 800 Nakanishi, M., & Niino, H. (2006). An improved mellor-yamada level-3 model: Its numerical  
801 stability and application to a regional prediction of advection fog. *Boundary-Layer*  
802 *Meteorology*, **119**(2), 397-407. <https://doi.org/10.1007/s10546-005-9030-8>
- 803 Nakanishi, M., & Niino, H. (2009). Development of an Improved Turbulence Closure Model  
804 for the Atmospheric Boundary Layer. *Journal of the Meteorological Society of Japan*,  
805 **87**(5), 895-912. <https://doi.org/10.2151/jmsj.87.895>
- 806 National Centers for Environmental Prediction/National Weather Service/NOAA/U.S.  
807 Department of Commerce (2000), NCEP FNL Operational Model Global Tropospheric  
808 Analyses, continuing from July 1999, <https://doi.org/10.5065/D6M043C6>, Research  
809 Data Archive at the National Center for Atmospheric Research, Computational and  
810 Information Systems Laboratory, Boulder, Colo. (Updated daily.) Accessed 22 Apr  
811 2019.



- 812 Petaja, T., Jarvi, L., Kerminen, V. M., Ding, A. J., Sun, J. N., Nie, W., et al. (2016). Enhanced  
813 air pollution via aerosol-boundary layer feedback in China. *Scientific Reports*, **6**.  
814 <https://doi.org/10.1038/srep18998>
- 815 Qi, Y. L., Ge, J. M., & Huang, J. P. (2013). Spatial and temporal distribution of MODIS and  
816 MISR aerosol optical depth over northern China and comparison with AERONET.  
817 *Chinese Science Bulletin*, **58**(20), 2497-2506. [https://doi.org/10.1007/s11434-013-](https://doi.org/10.1007/s11434-013-5678-5)  
818 [5678-5](https://doi.org/10.1007/s11434-013-5678-5)
- 819 Rinke, A., Dethloff, K., & Fortmann, M. (2004). Regional climate effects of Arctic Haze.  
820 *Geophysical Research Letters*, **31**(16). <https://doi.org/10.1029/2004gl020318>
- 821 Rosenfeld, D., Lohmann, U., Raga, G. B., O'Dowd, C. D., Kulmala, M., Fuzzi, S., et al. (2008).  
822 Flood or drought: How do aerosols affect precipitation? *Science*, **321**(5894), 1309-1313.  
823 <https://doi.org/10.1126/science.1160606>
- 824 Rosenfeld, D., Andreae, M. O., Asmi, A., Chin, M., de Leeuw, G., Donovan, D. P., et al. (2014).  
825 Global observations of aerosol-cloud-precipitation-climate interactions. *Reviews of*  
826 *Geophysics*, **52**(4), 750-808. <https://doi.org/10.1002/2013rg000441>
- 827 Skamarock, W. C., J. B. Klemp, J. Dudhia, D. O. Gill, D. M. Barker, M. G. Duda, W. Wang,  
828 and J. G. Powers (2008), A description of the advanced research WRF version 3, NCAR  
829 Tech. Note NCAR/TN-4751STR, 113 pp., Boulder, Colo.
- 830 Schwartz, S. E. (1996). The Whitehouse effect - Shortwave radiative forcing of climate by  
831 anthropogenic aerosols: An overview. *Journal of Aerosol Science*, **27**(3), 359-382.  
832 [https://doi.org/10.1016/0021-8502\(95\)00533-1](https://doi.org/10.1016/0021-8502(95)00533-1)
- 833 Seth, A., & Giorgi, F. (1998). The effects of domain choice on summer precipitation simulation  
834 and sensitivity in a regional climate model. *Journal of Climate*, **11**(10), 2698-2712.  
835 [https://doi.org/10.1175/1520-0442\(1998\)011<2698:Teodco>2.0.Co;2](https://doi.org/10.1175/1520-0442(1998)011<2698:Teodco>2.0.Co;2)
- 836 Song, F. F., & Zhou, T. J. (2014). The Climatology and Interannual Variability of East Asian  
837 Summer Monsoon in CMIP5 Coupled Models: Does Air-Sea Coupling Improve the  
838 Simulations? *Journal of Climate*, **27**(23), 8761-8777. [https://doi.org/10.1175/Jcli-D-](https://doi.org/10.1175/Jcli-D-14-00396.1)  
839 [14-00396.1](https://doi.org/10.1175/Jcli-D-14-00396.1)
- 840 Song, F. F., Zhou, T. J., & Qian, Y. (2014). Responses of East Asian summer monsoon to  
841 natural and anthropogenic forcings in the 17 latest CMIP5 models. *Geophysical*  
842 *Research Letters*, **41**(2), 596-603. <https://doi.org/10.1002/2013gl058705>
- 843 Tao, W. K., Chen, J. P., Li, Z. Q., Wang, C., & Zhang, C. D. (2012). Impact of Aerosols on  
844 Convective Clouds and Precipitation. *Reviews of Geophysics*, **50**.  
845 <https://doi.org/10.1029/2011rg000369>



- 846 Twomey, S. (1977). The influence of pollution on the shortwave albedo of clouds. *Journal of*  
847 *the Atmospheric Sciences*, **34**, 1149-1152. <https://doi.org/10.1175/1520->  
848 [0469\(1977\)034<1149:TIOPOT>2.0.CO;2](https://doi.org/10.1175/1520-0469(1977)034<1149:TIOPOT>2.0.CO;2)
- 849 Wang, B., & Yang, H. W. (2008). Hydrological issues in lateral boundary conditions for  
850 regional climate modeling: simulation of east asian summer monsoon in 1998. *Climate*  
851 *Dynamics*, **31**(4), 477-490. <https://doi.org/10.1007/s00382-008-0385-7>
- 852 Wang, Q. Y., Wang, Z. L., & Zhang, H. (2017). Impact of anthropogenic aerosols from global,  
853 East Asian, and non-East Asian sources on East Asian summer monsoon system.  
854 *Atmospheric Research*, **183**, 224-236. <https://doi.org/10.1016/j.atmosres.2016.08.023>
- 855 Wang, T., Wang, H. J., Ottera, O. H., Gao, Y. Q., Suo, L. L., Furevik, T., & Yu, L. (2013).  
856 Anthropogenic agent implicated as a prime driver of shift in precipitation in eastern  
857 China in the late 1970s. *Atmospheric Chemistry and Physics*, **13**(24), 12433-12450.  
858 <https://doi.org/10.5194/acp-13-12433-2013>
- 859 Wang, T. J., Zhuang, B. L., Li, S., Liu, J., Xie, M., Yin, C. Q., et al. (2015). The interactions  
860 between anthropogenic aerosols and the East Asian summer monsoon using RegCCMS.  
861 *Journal of Geophysical Research-Atmospheres*, **120**(11), 5602-5621.  
862 <https://doi.org/10.1002/2014jd022877>
- 863 Warner, T. T., Peterson, R. A., & Treadon, R. E. (1997). A tutorial on lateral boundary  
864 conditions as a basic and potentially serious limitation to regional numerical weather  
865 prediction. *Bulletin of the American Meteorological Society*, **78**(11), 2599-2617.  
866 [https://doi.org/10.1175/1520-0477\(1997\)078<2599:Atolbc>2.0.Co;2](https://doi.org/10.1175/1520-0477(1997)078<2599:Atolbc>2.0.Co;2)
- 867 Wiedinmyer, C., Akagi, S. K., Yokelson, R. J., Emmons, L. K., Al-Saadi, J. A., Orlando, J. J.,  
868 & Soja, A. J. (2011). The Fire INventory from NCAR (FINN): a high resolution global  
869 model to estimate the emissions from open burning. *Geoscientific Model Development*,  
870 **4**(3), 625-641. <https://doi.org/10.5194/gmd-4-625-2011>
- 871 Wu, G. X., Li, Z. Q., Fu, C. B., Zhang, X. Y., Zhang, R. Y., Zhang, R. H., et al. (2016).  
872 Advances in studying interactions between aerosols and monsoon in China. *Science*  
873 *China-Earth Sciences*, **59**(1), 1-16. <https://doi.org/10.1007/s11430-015-5198-z>
- 874 Wu, L. T., Su, H., & Jiang, J. H. (2013). Regional simulation of aerosol impacts on precipitation  
875 during the East Asian summer monsoon. *Journal of Geophysical Research-*  
876 *Atmospheres*, **118**(12), 6454-6467. <https://doi.org/10.1002/jgrd.50527>
- 877 Xiao, Z. X., & Duan, A. M. (2016). Impacts of Tibetan Plateau Snow Cover on the Interannual  
878 Variability of the East Asian Summer Monsoon. *Journal of Climate*, **29**(23), 8495-8514.  
879 <https://doi.org/10.1175/Jcli-D-16-0029.1>



- 880 Xie, X., Wang, H., Liu, X., Li, J., Wang, Z., & Liu, Y. (2016). Distinct effects of anthropogenic  
881 aerosols on the East Asian summermonsoon between multidecadal strong and  
882 weakmonsoon stages. *Journal of Geophysical Research-Atmospheres*, **121**(12), 7026-  
883 7040. <https://doi.org/10.1002/2015jd024228>
- 884 Xue, Y. K., Janjic, Z., Dudhia, J., Vasic, R., & De Sales, F. (2014). A review on regional  
885 dynamical downscaling in intraseasonal to seasonal simulation/prediction and major  
886 factors that affect downscaling ability. *Atmospheric Research*, **147**, 68-85.  
887 <https://doi.org/10.1016/j.atmosres.2014.05.001>
- 888 Yan, H. P., Qian, Y., Zhao, C., Wang, H. L., Wang, M. H., Yang, B., et al. (2015). A new  
889 approach to modeling aerosol effects on East Asian climate: Parametric uncertainties  
890 associated with emissions, cloud microphysics, and their interactions. *Journal of*  
891 *Geophysical Research-Atmospheres*, **120**(17), 8905-8924.  
892 <https://doi.org/10.1002/2015jd023442>
- 893 Zaveri, R. A., Easter, R. C., Fast, J. D., & Peters, L. K. (2008). Model for Simulating Aerosol  
894 Interactions and Chemistry (MOSAIC). *Journal of Geophysical Research-Atmospheres*,  
895 **113**(D13). <https://doi.org/10.1029/2007jd008782>
- 896 Zaveri, R. A., & Peters, L. K. (1999). A new lumped structure photochemical mechanism for  
897 large-scale applications. *Journal of Geophysical Research-Atmospheres*, **104**(D23),  
898 30387-30415. <https://doi.org/10.1029/1999jd900876>
- 899 Zhang, M. X., Zhao, C., Cong, Z. Y., Du, Q. Y., Xu, M. Y., Chen, Y., et al. (2020). Impact of  
900 topography on black carbon transport to the southern Tibetan Plateau during the pre-  
901 monsoon season and its climatic implication. *Atmospheric Chemistry and Physics*,  
902 **20**(10), 5923-5943. <https://doi.org/10.5194/acp-20-5923-2020>
- 903 Zhang, H., Wang, Z. L., Wang, Z. Z., Liu, Q. X., Gong, S. L., Zhang, X. Y., et al. (2012).  
904 Simulation of direct radiative forcing of aerosols and their effects on East Asian climate  
905 using an interactive AGCM-aerosol coupled system. *Climate Dynamics*, **38**(7-8), 1675-  
906 1693. <https://doi.org/10.1007/s00382-011-1131-0>
- 907 Zhang, R. H. (2015). Changes in East Asian summer monsoon and summer rainfall over eastern  
908 China during recent decades. *Science Bulletin*, **60**(13), 1222-1224.  
909 <https://doi.org/10.1007/s11434-015-0824-x>
- 910 Zhang, X. Y., Wang, Y. Q., Niu, T., Zhang, X. C., Gong, S. L., Zhang, Y. M., & Sun, J. Y.  
911 (2012). Atmospheric aerosol compositions in China: spatial/temporal variability,  
912 chemical signature, regional haze distribution and comparisons with global aerosols.



- 913            *Atmospheric Chemistry and Physics*, **12**(14), 6273-6273. <https://doi.org/10.5194/acp-914-6273-2012>
- 915    Zhao, B., Liou, K. N., Gu, Y., Li, Q. B., Jiang, J. H., Su, H., et al. (2017). Enhanced PM<sub>2.5</sub>  
916            pollution in China due to aerosol-cloud interactions. *Scientific Reports*, **7**.  
917            <https://doi.org/10.1038/s41598-017-04096-8>
- 918    Zhao, C., Liu, X., Leung, L. R., Johnson, B., McFarlane, S. A., Gustafson, W. I., et al. (2010).  
919            The spatial distribution of mineral dust and its shortwave radiative forcing over North  
920            Africa: modeling sensitivities to dust emissions and aerosol size treatments.  
921            *Atmospheric Chemistry and Physics*, **10**(18), 8821-8838. <https://doi.org/10.5194/acp-922-10-8821-2010>
- 923    Zhao, C., Liu, X., Leung, L. R., & Hagos, S. (2011). Radiative impact of mineral dust on  
924            monsoon precipitation variability over West Africa. *Atmospheric Chemistry and*  
925            *Physics*, **11**(5), 1879-1893. <https://doi.org/10.5194/acp-11-1879-2011>
- 926    Zhao, C., Liu, X., & Leung, L. R. (2012). Impact of the Desert dust on the summer monsoon  
927            system over Southwestern North America. *Atmospheric Chemistry and Physics*, **12**(8),  
928            3717-3731. <https://doi.org/10.5194/acp-12-3717-2012>
- 929    Zhao, C., Chen, S., Leung, L. R., Qian, Y., Kok, J. F., Zaveri, R. A., & Huang, J. (2013a).  
930            Uncertainty in modeling dust mass balance and radiative forcing from size  
931            parameterization. *Atmospheric Chemistry and Physics*, **13**(21), 10733-10753.  
932            <https://doi.org/10.5194/acp-13-10733-2013>
- 933    Zhao, C., Leung, L. R., Easter, R., Hand, J., & Avise, J. (2013b). Characterization of speciated  
934            aerosol direct radiative forcing over California. *Journal of Geophysical Research-*  
935            *Atmospheres*, **118**(5), 2372-2388. <https://doi.org/10.1029/2012jd018364>
- 936    Zhao, C., Hu, Z., Qian, Y., Leung, L. R., Huang, J., Huang, M., et al. (2014). Simulating black  
937            carbon and dust and their radiative forcing in seasonal snow: a case study over North  
938            China with field campaign measurements. *Atmospheric Chemistry and Physics*, **14**(20),  
939            11475-11491. <https://doi.org/10.5194/acp-14-11475-2014>
- 940    Zhao, C., Huang, M. Y., Fast, J. D., Berg, L. K., Qian, Y., Guenther, A., et al. (2016).  
941            Sensitivity of biogenic volatile organic compounds to land surface parameterizations  
942            and vegetation distributions in California. *Geoscientific Model Development*, **9**(5),  
943            1959-1976. <https://doi.org/10.5194/gmd-9-1959-2016>
- 944    Zheng, B., Tong, D., Li, M., Liu, F., Hong, C. P., Geng, G. N., et al. (2018). Trends in China's  
945            anthropogenic emissions since 2010 as the consequence of clean air actions.



- 946           *Atmospheric Chemistry and Physics*, **18**(19), 14095-14111.  
947           <https://doi.org/10.5194/acp-18-14095-2018>
- 948   Zhou, T. J., Gong, D. Y., Li, J., & Li, B. (2009). Detecting and understanding the multi-decadal  
949           variability of the East Asian Summer Monsoon - Recent progress and state of affairs.  
950           *Meteorologische Zeitschrift*, **18**(4), 455-467. [https://doi.org/10.1127/0941-](https://doi.org/10.1127/0941-2948/2009/0396)  
951           2948/2009/0396
- 952   Zhu, Y. L., Wang, H. J., Zhou, W., & Ma, J. H. (2011). Recent changes in the summer  
953           precipitation pattern in East China and the background circulation. *Climate Dynamics*,  
954           **36**(7-8), 1463-1473. <https://doi.org/10.1007/s00382-010-0852-9>
- 955   Zhuang, B. L., Li, S., Wang, T. J., Liu, J., Chen, H. M., Chen, P. L., et al. (2018). Interaction  
956           between the Black Carbon Aerosol Warming Effect and East Asian Monsoon Using  
957           RegCM4. *Journal of Climate*, **31**(22), 9367-9388. [https://doi.org/10.1175/Jcli-D-17-](https://doi.org/10.1175/Jcli-D-17-0767.1)  
958           0767.1
- 959  
960  
961



962  
963  
964  
965  
966

**Table 1.** Experiment Description.

Experiment ID	Experiment Description
CTRL-L	Control experiment with large simulation domain.
CLEAN-L	Same as CTRL-L, but the anthropogenic aerosol emissions are 0.1 times of CTRL-L.
CTRL-S	Control experiment with small simulation domain.
CLEAN-S	Same as CTRL-S, but the anthropogenic aerosol emissions are 0.1 times of CTRL-S.

967  
968  
969  
970  
971  
972

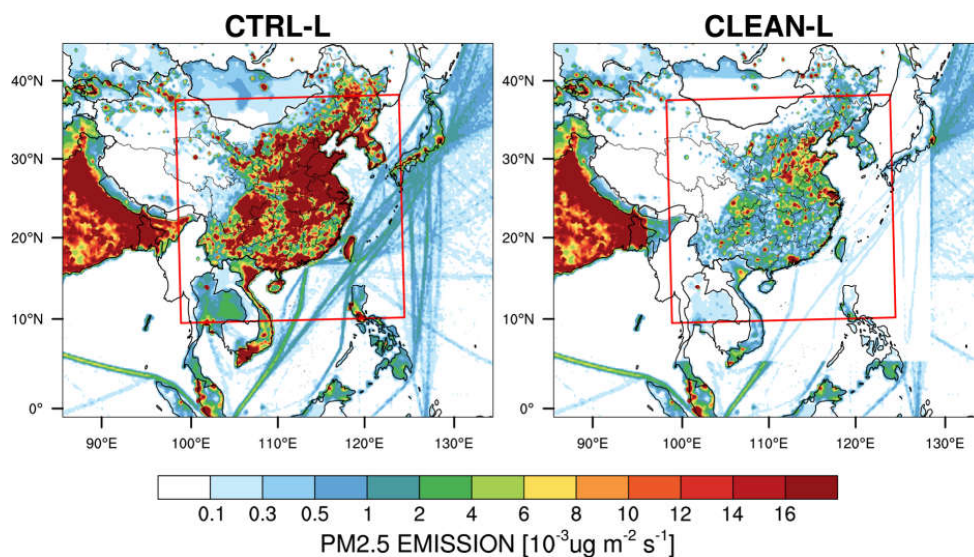
**Table 2.** Summary of model configurations.

Description	Selection(L, S)
Horizontal grid spacing	30km
Grid dimensions	201x231, 121x121
Vertical layers	41
Topography	USGS_30s
Model top press	100hPa
Aerosol scheme	MOSAIC 4 bin
Gas-phase chemistry	CBM-Z
Long wave Radiation	RRTMG
Short wave Radiation	RRTMG
Cloud Microphysics	Morrison 2-moment
Cumulus Cloud	Kain-Fritsch
Planetary boundary layer	MYNN 3rd
Land surface	unified Noah land-surface model
Meteorological Forcing	FNL, 1°x1° ,6 hourly

973  
974  
975  
976  
977  
978



979  
980  
981  
982  
983



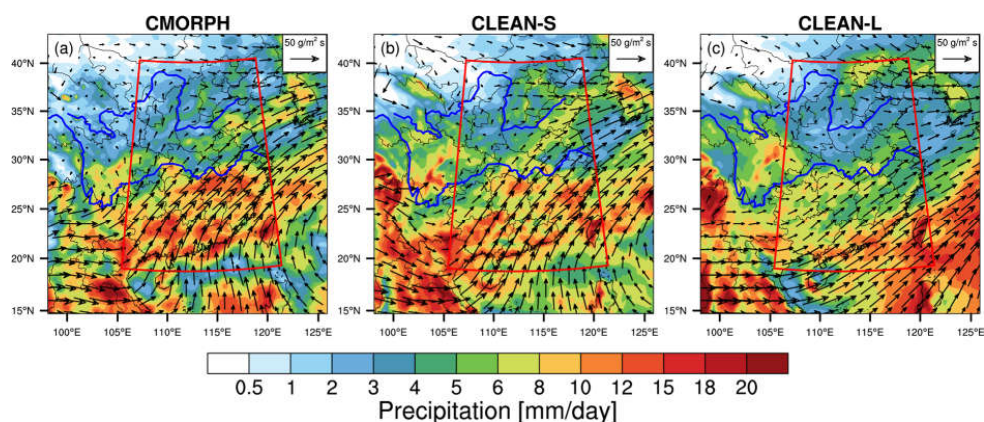
984  
985 **Figure 1.** Spatial distributions of anthropogenic emissions of primary PM2.5 averaged for June  
986 and July for the simulation domains. The red box in the large simulation domain represents the  
987 small domain.

988  
989  
990  
991  
992  
993  
994  
995  
996  
997  
998  
999  
1000  
1001  
1002  
1003  
1004  
1005





1006  
1007  
1008  
1009

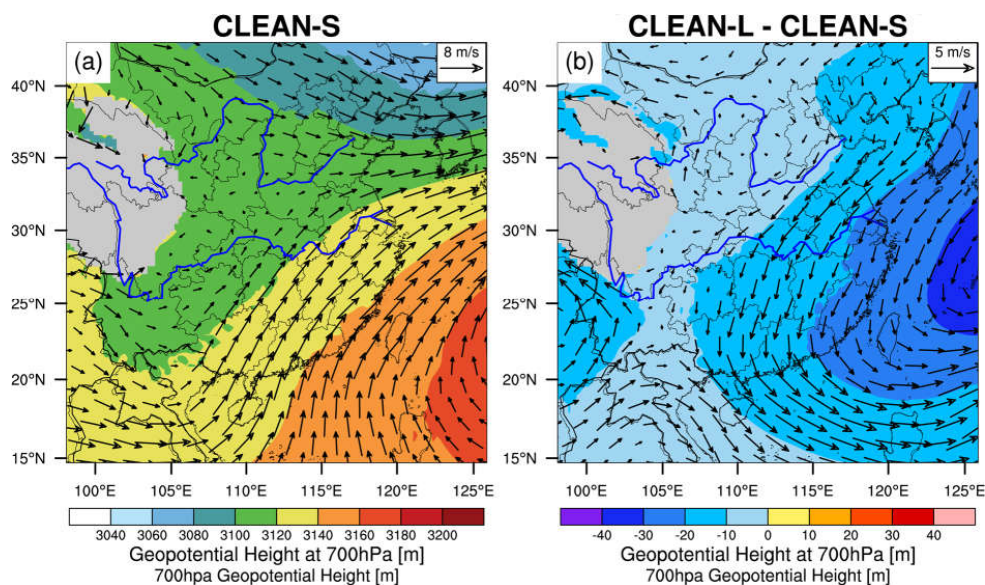


1010  
1011  
1012  
1013  
1014  
1015  
1016  
1017  
1018  
1019  
1020  
1021  
1022  
1023  
1024  
1025  
1026  
1027  
1028  
1029  
1030  
1031  
1032  
1033  
1034  
1035  
1036

**Figure 2.** Mean precipitation rate (mm/day) and 700hPa moisture transport ( $\text{g/m}^2 \text{s}$ ) over the small domain for the two months of June and July 2017 from (a) CMORPH and ERA5 reanalysis, (b) CLEAN-S simulation, and (c) CLEAN-L simulation. The red box ( $20^\circ\text{N}$ - $42^\circ\text{N}$ ,  $105^\circ\text{E}$ - $122^\circ\text{E}$ ) represents the focus area of analysis in follow. (a) Precipitation data comes from CMORPH, and the 700hPa moisture transport field data is obtained by processing ERA5 reanalysis.



1037  
1038  
1039  
1040  
1041  
1042

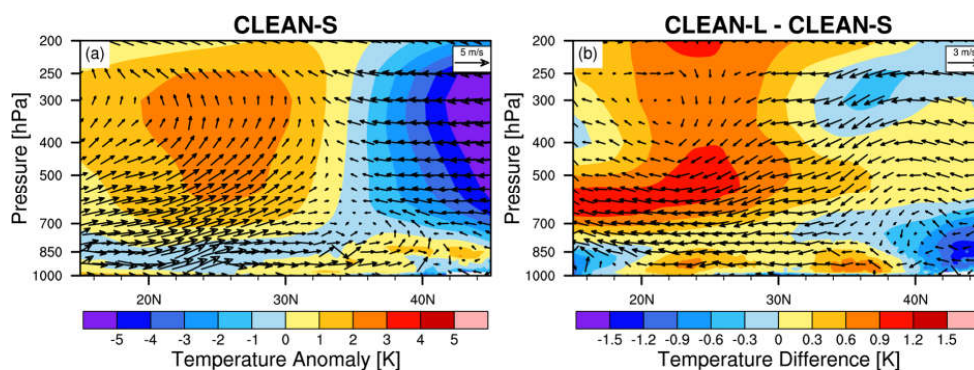


1043 **Figure 3.** Spatial distribution of mean 700 hPa Geopotential Height and winds of June and  
1044 July 2017 from (a) CLEAN-S, and the (b) difference between CLEAN-L and CLEAN-S.

1045  
1046  
1047  
1048  
1049  
1050  
1051  
1052  
1053  
1054  
1055  
1056  
1057  
1058  
1059  
1060  
1061  
1062  
1063



1064  
1065  
1066  
1067  
1068  
1069

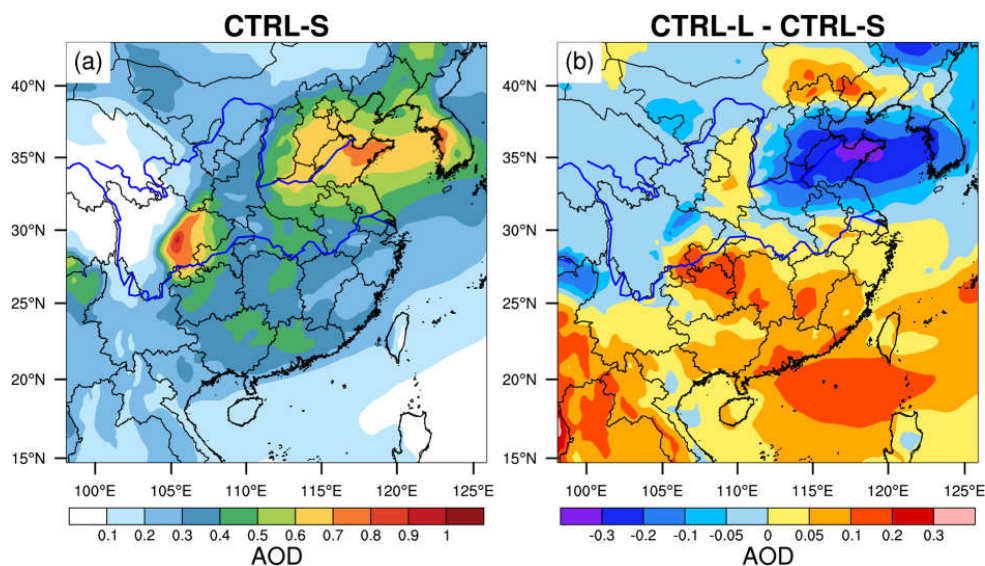


1070  
1071  
1072  
1073  
1074  
1075  
1076  
1077  
1078  
1079  
1080  
1081  
1082  
1083  
1084  
1085  
1086  
1087  
1088  
1089  
1090  
1091  
1092  
1093  
1094  
1095

**Figure 4.** The cross-section of meridional temperature anomalies and wind averaged for 105°E and 122°E from (a) the CLEAN-S simulation, and (b) the difference of temperature (not meridional temperature anomalies) between CLEAN-L and CLEAN-S. The meridional temperature anomalies are calculated by subtracting the mean temperature in this latitude range at each pressure level.



1096  
1097  
1098  
1099  
1100  
1101  
1102

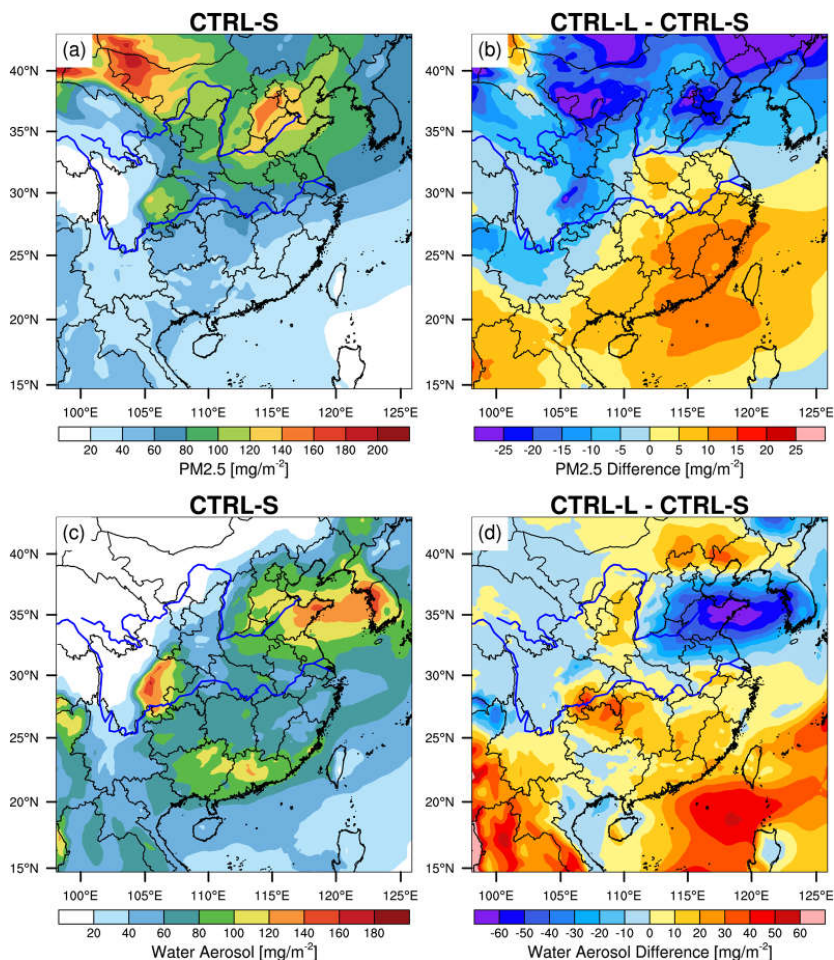


1103  
1104  
1105  
1106  
1107  
1108  
1109  
1110  
1111  
1112  
1113  
1114  
1115  
1116  
1117  
1118  
1119  
1120  
1121

**Figure 5.** The spatial distribution of AOD for June and July of 2017 from the CTRL-S simulation, and the difference between CTRL-L and CTRL-S.



1122  
1123  
1124

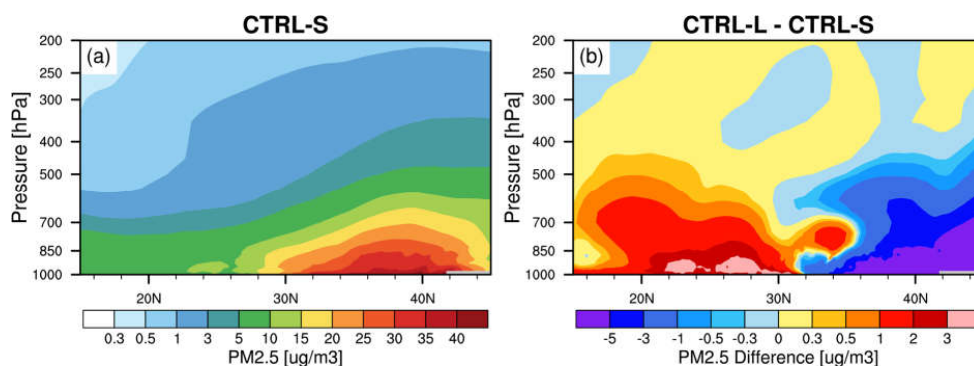


1125  
1126  
1127  
1128  
1129  
1130  
1131  
1132  
1133  
1134  
1135  
1136  
1137

**Figure 6.** The spatial distributions of column integrated total (a) PM<sub>2.5</sub> concentration and (c) water content in aerosol averaged for June and July of 2017 from the CTRL-S simulation, and (b) (d) the difference between CTRL-L and CTRL-S.



1138  
1139  
1140  
1141  
1142  
1143  
1144  
1145

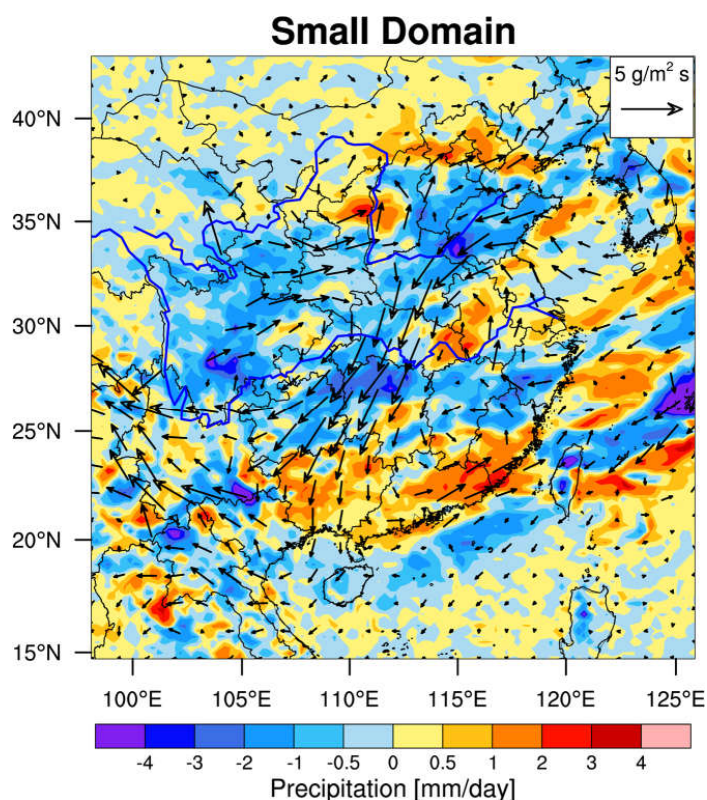


1146  
1147 **Figure 7.** The latitude-height cross-section of (a) total PM2.5 averaged between 105°E and  
1148 122°E for June and July of 2017 from the CTRL-S experiment, and (b) the difference between  
1149 CTRL-L and CTRL-S.

1150  
1151  
1152  
1153  
1154  
1155  
1156  
1157  
1158  
1159  
1160  
1161  
1162  
1163  
1164  
1165  
1166  
1167  
1168  
1169  
1170  
1171



1172  
1173  
1174  
1175  
1176  
1177  
1178

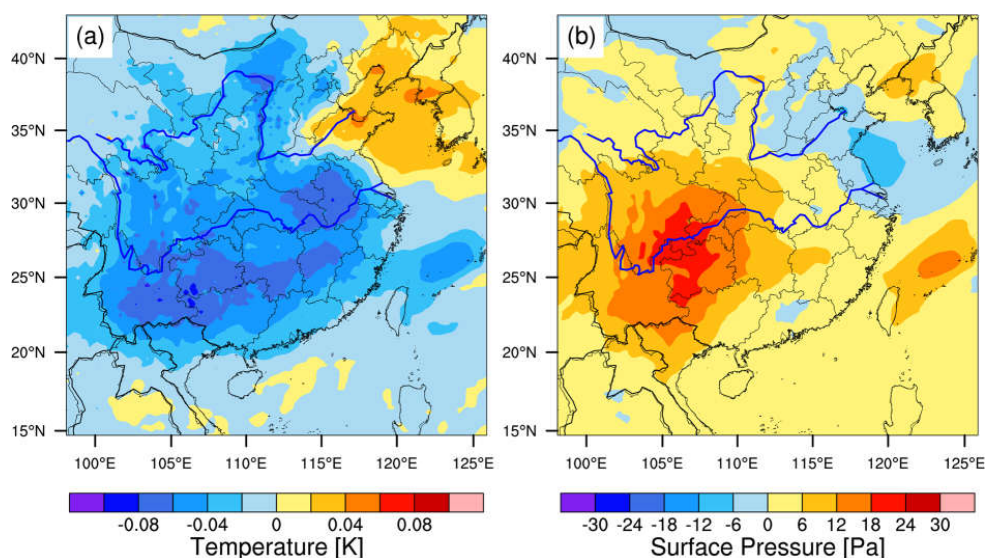


1179  
1180 **Figure 8.** The spatial distributions of aerosol-induced difference (CTRL-CLEAN) of  
1181 precipitation and moisture transport at 700 hPa averaged for June and July of 2017 from the  
1182 small domain simulations.

1183  
1184  
1185  
1186  
1187  
1188  
1189  
1190  
1191  
1192  
1193  
1194



1195  
1196  
1197  
1198  
1199  
1200  
1201  
1202  
1203  
1204



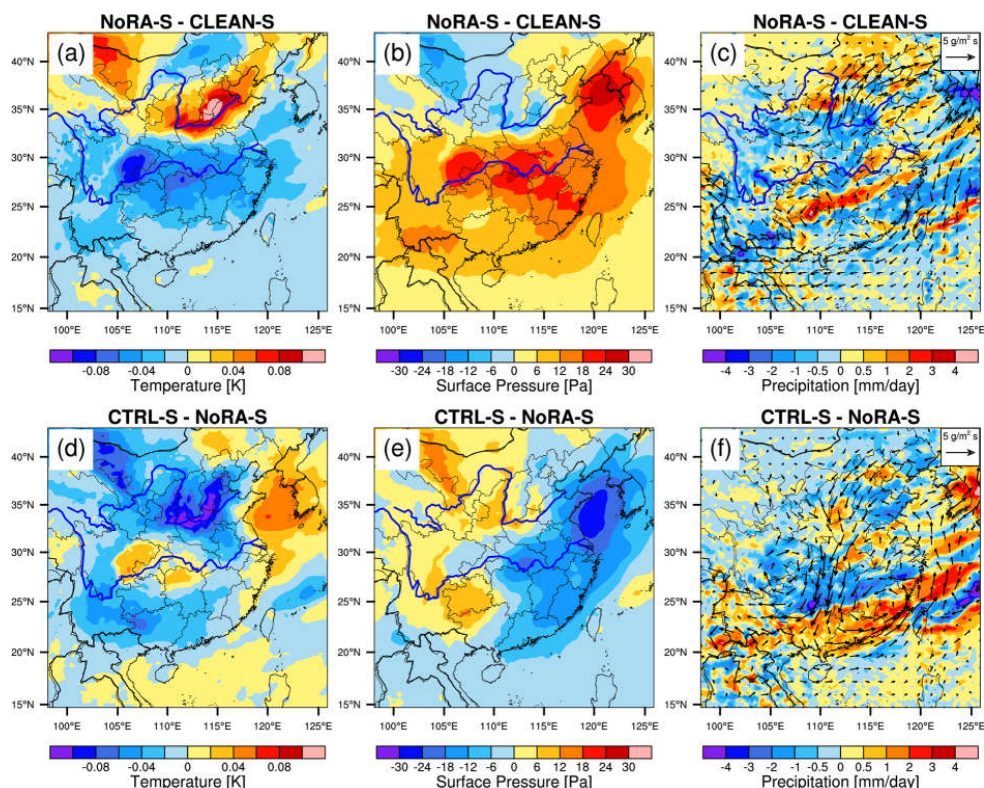
1205  
1206  
1207  
1208  
1209  
1210  
1211  
1212  
1213  
1214  
1215  
1216  
1217  
1218  
1219  
1220  
1221  
1222  
1223  
1224  
1225  
1226  
1227

**Figure 9.** The spatial distributions of aerosol-induced difference (CTRL-CLEAN) of (a) atmosphere temperature below 500 hPa and (b) surface pressure averaged for June and July of 2017 from the small domain simulations. We interpolate the atmosphere temperature to the isobaric surface below 500 hPa and get the atmosphere temperature below 500 hPa by weighted average according to the layer height.





1228  
1229  
1230  
1231  
1232

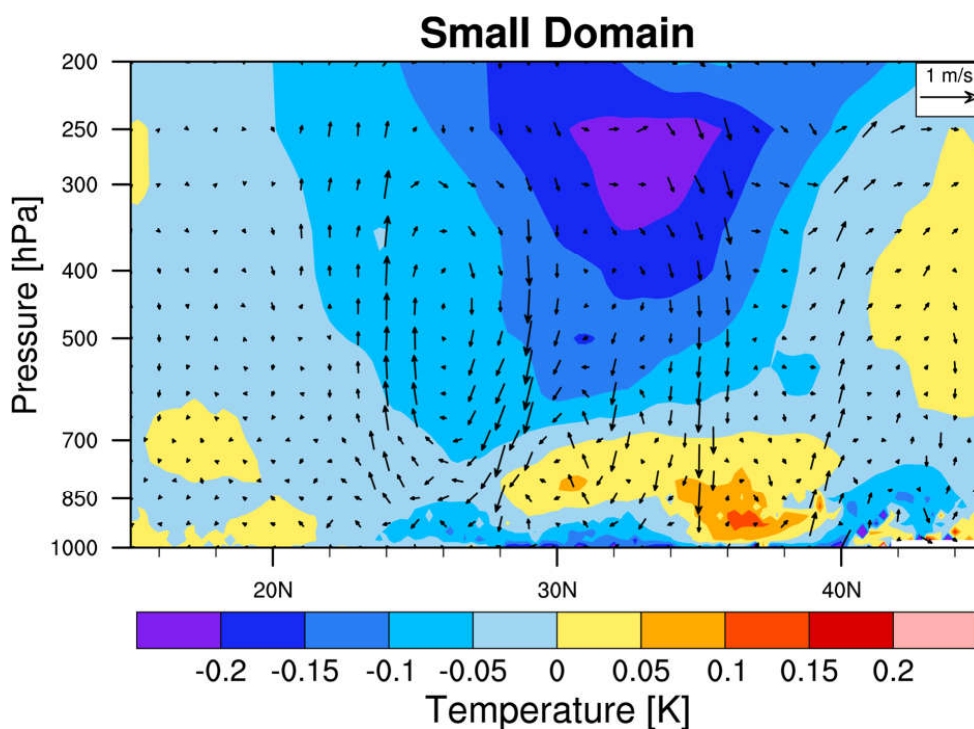


1233  
1234  
1235  
1236  
1237  
1238  
1239  
1240  
1241  
1242  
1243  
1244  
1245  
1246  
1247  
1248  
1249  
1250  
1251  
1252

**Figure 10.** The spatial distributions of Aerosol-Cloud interactions induced difference of (a) atmosphere temperature below 500 hPa, (b) surface pressure and (c) precipitation and moisture transport at 700 hPa averaged for June and July of 2017 from the small domain simulations. And the spatial distributions of Aerosol-Radiation interactions induced difference of (d) atmosphere temperature below 500 hPa, (e) surface pressure and (f) precipitation and moisture transport at 700 hPa averaged for June and July of 2017 from the small domain simulations.



1253  
1254  
1255  
1256  
1257

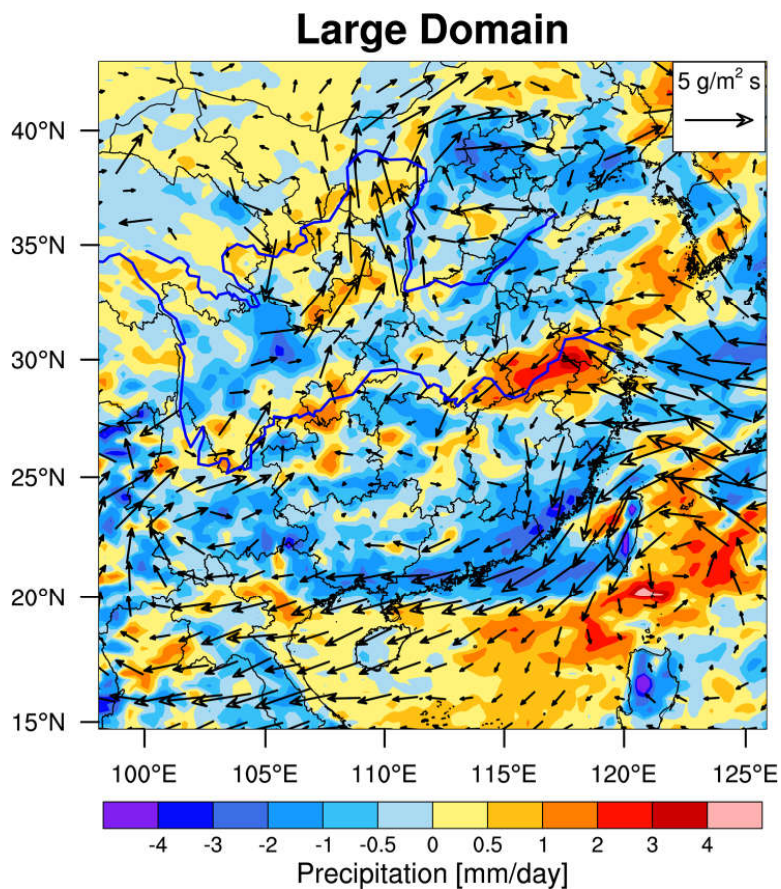


1258  
1259  
1260  
1261  
1262  
1263  
1264  
1265  
1266  
1267  
1268  
1269  
1270  
1271  
1272  
1273  
1274  
1275  
1276  
1277  
1278  
1279

**Figure 11.** The latitude-pressure cross-section of aerosol-induced difference (CTRL-CLEAN) of temperature and wind averaged between 105°E and 122°E for June and July of 2017 from the small domain simulation.



1280  
1281  
1282  
1283

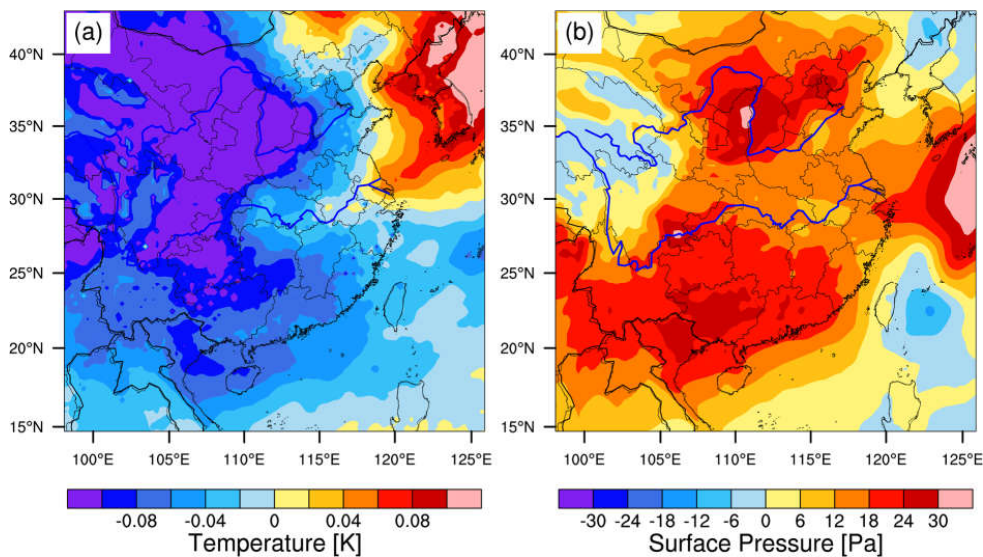


1284  
1285  
1286  
1287  
1288  
1289  
1290  
1291  
1292  
1293  
1294  
1295  
1296  
1297  
1298

**Figure 12.** The same as figure 8, but from the large domain simulation.



1299  
1300  
1301  
1302  
1303  
1304

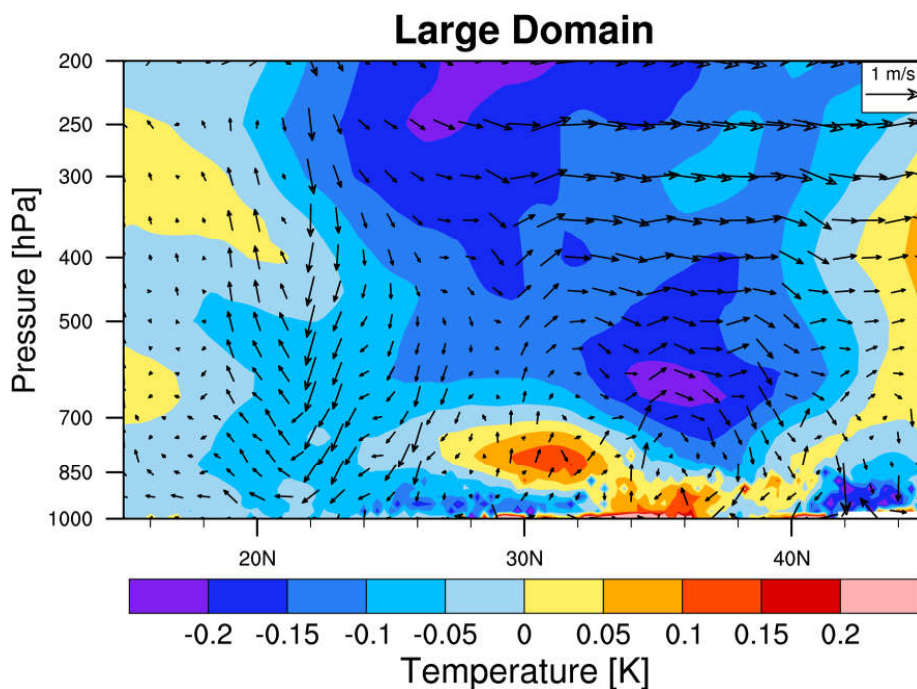


1305  
1306  
1307  
1308  
1309  
1310  
1311  
1312  
1313  
1314  
1315  
1316  
1317  
1318  
1319  
1320  
1321  
1322  
1323  
1324  
1325  
1326

**Figure 13.** Same as Fig. 9, but from the large domain simulation.



1327  
1328  
1329  
1330  
1331

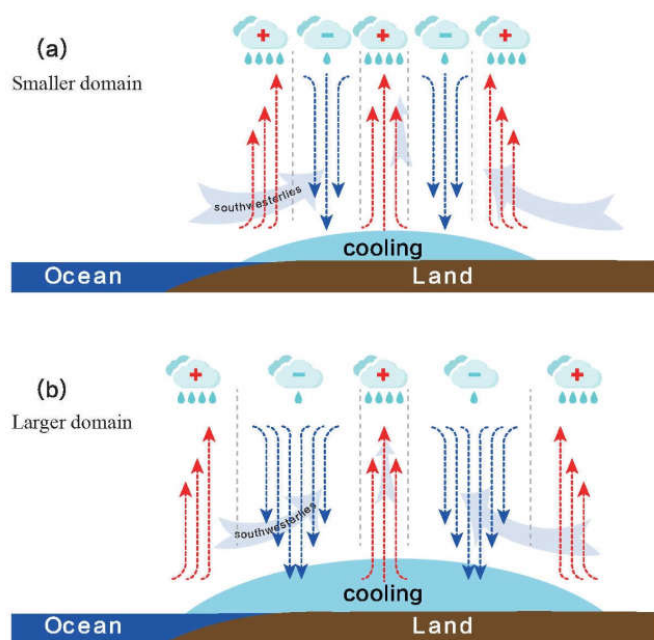


1332  
1333  
1334  
1335  
1336  
1337  
1338  
1339  
1340  
1341  
1342  
1343  
1344  
1345  
1346  
1347  
1348

**Figure 14.** Same as figure 11, but from the large domain simulation.



1349  
1350  
1351  
1352



1353  
1354  
1355  
1356  
1357  
1358  
1359

**Figure 15.** The schematic plot of aerosol impacts in (a) small domain simulation and (b) large domain simulation over East Asia. The light blue shadow area represents the extent of aerosol induced decrease of lower tropospheric temperature and increase of surface pressure. The red (blue) vector dash lines represent updraft (downdraft) anomalies. The “+” (“-”) above the region indicates the aerosol-induced increase (decrease) of precipitation.